Universidade do Minho
Escola de Engenharia
Instituto de Investigação em Biomateriais,
Biodegradáveis e Biomiméticos

Filipa Isabel Rafael Bastos

Inorganic-templated and polymeric layer-by-layer nanocapsules for the treatment of cancer

January 2023

Inorganic-templated and polymeric layer-by-layer nanocapsules for the treatment of cancer
Filipa Bastos
UMinho | 2023

Universidade do Minho
Escola de Engenharia
Instituto de Investigação em Biomateriais,
Biodegradáveis e Biomiméticos

Filipa Isabel Rafael Bastos

Inorganic-templated and polymeric layer-by-layer nanocapsules for the treatment of cancer

Master Thesis

Master's degree in Biomedical Engineering

Dissertation supervised by:

Natália Maria de Araújo Alves

Iva Hristova Pashkuleva

January 2023

DECLARATION

Name: Filipa Isabel Rafael Bastos
Project Title: Inorganic-templated and polymeric layer-by-layer nanocapsules for the treatment of cancer
Mentors: Natália Maria de Araújo Alves; Iva Hristova Pashkuleva
Conclusion Year: 2023
Master Designation: Mestrado Integrado em Engenharia Biomédica
Master Branch: Biomateriais, Reabilitação e Biomecânica

Universidade do Minho, 31/01/2023

Signature: Filipa Bastos

AGRADECIMENTOS

Esta dissertação representa o fim de um ciclo. “Estes anos são viagem” e várias pessoas se cruzaram nela, fazendo desta viagem a mais incrível de sempre. Dessa forma, não podia encerrar este ciclo sem antes lhes agradecer.

Em primeiro lugar, gostaria de agradecer ao Professor Rui Reis pela oportunidade e privilégio de desenvolver a minha dissertação de mestrado no Instituto de Investigação em Biomateriais, Biodegradáveis e Biomiméticos (I3Bs), na Universidade do Minho.

Agradeço à minha orientadora, Professora Natália Alves, por toda a ajuda e pela disponibilidade de desenvolver esta dissertação sob sua orientação. Muito obrigada pela oportunidade de ganhar experiência na área de investigação, pela dedicação e por todo o tempo dispensado!

À minha coorientadora, Iva Pashkuleva, por todo o conhecimento transmitido, pelos conselhos e por toda a ajuda ao longo desta dissertação. Muito obrigada pela disponibilidade e pela oportunidade de poder integrar o seu grupo de investigação!

Ao Rui Costa e à Diana Costa, por toda a ajuda no laboratório, bem como na análise de resultados. Obrigada pela paciência, tiveram um papel bastante importante nesta etapa e sem vocês não teria conseguido.

À antiga Library Crew e agora aos novos “Arrumos”, estou eternamente grata por estarem sempre presentes. Por todas as palavras de motivação, por todos os momentos divertidos e por alegrarem sempre os dias menos bons. Por sentirem este meu fim de ciclo, como se fosse o vosso. Obrigada por serem quem são, foi uma sorte ter-vos conhecido. Que isto seja apenas um até já e nunca um adeus.

À Crop, por todo o apoio que me deu, por todas as palavras, por estar sempre lá quando tudo parecia difícil, nas vitórias e nas derrotas. Por todos os momentos que passámos ao longo destes 5 anos. Contigo estes anos foram uma viagem da qual eu sempre me vou lembrar.

Ao Tiago, por estar sempre ao meu lado e me transmitir paz quando tudo parecia desabar. Obrigada, também à sua família por sempre me ouvirem com interesse a falar do tema, mesmo sem entenderem do que falava. Obrigada por todo o apoio e por me ajudarem a acreditar que conseguia tudo, mesmo quando eu própria não acreditava em mim!

E por fim, à minha família, em especial à minha mãe, por ter sido uma fonte de inspiração durante toda esta dissertação. Por todo o esforço que fez para que nunca me faltasse nada para alcançar tudo o que alcancei até hoje. À minha avó e à minha irmã por todas as palavras de força. Também ao meu pai, que apesar de já ter partido, sei que estaria muito orgulhoso de mim.

Foram 5 anos com altos e baixos, com muitas dúvidas e incertezas. É com nostalgia que hoje termino com a certeza de que este percurso não poderia ter sido melhor. Por todas as pessoas que por ele passaram, por todas as aprendizagens, por todos os obstáculos. Um muito obrigada!

STATEMENT OF INTEGRITY

I hereby declare having conducted this academic work with integrity. I confirm that I have not used plagiarism or any form of undue use of information or falsification of results along the process leading to its elaboration.
I further declare that I have fully acknowledged the Code of Ethical Conduct of the University of Minho.

Universidade do Minho, 31/01/2023

Signature: Filipa Bastos

ABSTRACT

Breast cancer is one of the most prevalent diseases worldwide and the most malignant in women. Conventional treatments include a radiotherapy, which kills both healthy and cancerous cells unselectively and chemotherapy, which is more selective but fails against aggressive tumors that present drug resistance. These limitations, together with their side effects and high tumor heterogeneity, are major obstacles to treatment efficacy. Therefore, it is important to develop new classes of carriers that can deliver anticancer agents to the tumor site, while minimizing the impact on healthy cells.

This project proposes a drug delivery system that involves several bioactive components to endow targeting capacity against cancer cells and *in situ* release of anticancer drugs. To this end, we will develop core/shell nanocapsules that are composed by calcium carbonate ($CaCO_3$) nanoparticles with capacity for loading chemotherapeutics, and a layer-by-layer (LbL) coating comprising ligands for receptors that are overexpressed by breast cancer cells. The work plan comprises: (i) synthesis of spherical $CaCO_3$ nanoparticles loaded with a model low molecular weight molecule (*i.e.*, rhodamine), (ii) coating the nanoparticles using the polycationic poly-L-lysine and the polyanionic hyaluronic acid (HA), the latter a known ligand that target CD44 receptors overexpressed in breast cancer cells, (iii) characterization of the loading efficiency and releasing profiles in an acidic buffer that simulates a tumor microenvironment, and (iv) *in vitro* impact on breast cancer cell lines with different metastatic potential – MDA-MB-231 and SK-BR-3. We expect that this project would contribute to the development of a new drug delivery system with an improved therapeutic response.

We were able to produce nanoparticles that enabled the deposition of an LbL coating that endowed CD44 targeting. Rhodamine was loaded as a model molecule to demonstrate a pH-dependent release from $CaCO_3$ nanoparticles. The breast cancer cells MDA-MB-231 (aggressive phenotype) and SK-BR-3 (less aggressive) showed a substantial immobilization of coated nanoparticles in the ECM compared with a control of healthy cells (MCF10A cells), consistent with the interaction of the HA in the coating with the CD44 receptors in the pericellular space and reduced metabolic activity. These findings also suggest that different receptors may mediate internalization instead of immobilization in the ECM, as our experiments showed that by blocking CD44 the nanoparticles entered the cells. These results demonstrate that LbL-coated $CaCO_3$ systems would be an excellent family of carriers for the transport of chemotherapeutics and localized delivery targeted at the tumor microenvironment.

Keywords: Layer-by-layer, drug delivery, breast cancer, calcium carbonate, bioactive components.

RESUMO

O cancro da mama é uma das doenças mais prevalentes em todo o mundo e a mais maligna, nas mulheres. Os tratamentos convencionais incluem a radioterapia, que mata células saudáveis e cancerígenas de forma não seletiva e a quimioterapia, que apesar de ser mais seletiva, falha contra tumores agressivos que apresentam resistência aos medicamentos. Estas limitações, juntamente com os seus efeitos secundários, constituem grandes obstáculos à eficácia do tratamento. Dessa forma, é importante desenvolver novos portadores que possam fornecer agentes anticancerígenos ao local do tumor, minimizando ao mesmo tempo o impacto nas células saudáveis.

Este projeto propõe um sistema de entrega de fármacos que envolve vários componentes bioativos com capacidade seletiva contra as células cancerígenas e a libertação *in situ* de agentes anticancerígenos. Para este fim, desenvolveremos nanocápsulas compostas por carbonato de cálcio ($CaCO_3$) com carregar agentes quimioterapêuticos, e um revestimento camada por camada, compreendendo ligandos para recetores que são sobreexpressos pelas células de cancro da mama. O plano de trabalho inclui: (i) síntese de nanopartículas esféricas de $CaCO_3$ carregadas com uma molécula modelo de baixo peso molecular (rodamina), (ii) revestimento das nanopartículas utilizando poli-lisina e ácido hialurónico cujo alvo são os recetores CD44, (iii) caracterização da eficiência do encapsulamento e perfis de libertação num tampão ácido que simula um microambiente tumoral, e (iv) impacto *in vitro* nas linhas celulares de cancro da mama com diferentes potenciais metastáticos.

Produzimos nanopartículas que permitiram o revestimento camada por camada, que interagiu com o alvo CD44. A rodamina foi encapsulada como uma molécula modelo para demonstrar a libertação dependente do pH das nanopartículas. As células de cancro da mama MDA-MB-231 (fenótipo agressivo) e SK-BR-3 (menos agressivo) mostraram uma imobilização substancial de nanopartículas revestidas, em comparação com o controlo de células saudáveis (MCF10A), consistente com a interação do HA no revestimento com os recetores CD44 no espaço pericelular, e uma atividade metabólica reduzida. Estas descobertas sugerem também que diferentes recetores podem mediar a internalização, uma vez que os nossos ensaios mostraram que, ao bloquear o CD44, as nanopartículas entraram nas células. Estes resultados demonstram que os sistemas $CaCO_3$ revestidos seriam um excelente candidato para o transporte de agentes anticancerígenos e entrega localizada direcionada para o microambiente tumoral.

Palavras-chave: camada por camada, libertação de fármacos, cancro da mama, carbonato de cálcio, componentes bioativos.

TABLE OF CONTENTS

List of Figures

Chapter 1- General Introduction

Chapter 2- Materials and Methods

CHAPTER 3- LAYER-BY-LAYER COATED CALCIUM CARBONATE NANOPARTICLES FOR THE TARGETING OF BREAST CANCER CELLS

LIST OF TABLES

CHAPTER 1- GENERAL INTRODUCTION

List of Abbreviations and acronyms

A

ADCs	Antibody-drug conjugates
AIs	Aromatase Inhibitors
ATCC	American Type Culture Collection

C

$CaCO_3$	Calcium Carbonate
$CaCl_2$	Calcium Chloride
CSCs	Cancer Stem Cells
Ch/ γ-PGA NPs	Chitosan/poly(γ-glutamic acid) nanoparticles
CD44	Cluster of differentiation 44
CoA	Coactivators
CoR	Corepressors
CLSM	Confocal laser scanning microscope

D

DDS	Drug Delivery System
DMEM	Dulbecco's Modified Eagle Medium
DNA	Deoxyribonucleic acid
DOX	Doxorubicin
DLS	Dynamic Laser Scattering

E

EG	Ethylene Glycol
ET	Endocrine Therapy
ER	Estrogen Receptor
ERE	Estrogen Response Elements
ECM	Extracellular matrix

F

FBS	Fetal bovine serum
FDA	Food and Drug Administration

H

Hep	Heparin
HA	Hyaluronic Acid
HCSL-NPs	Histidine-grafted Cchitosan-lipoic acid nanoparticles
HR	Hormone Receptor

HER2	Human epidermal growth factor receptor 2
HCl	Hydrochloric acid

I

IONPs	Iron Oxide Nanoparticles

K

KCl	Potassium Chloride

L

LbL	Layer-by-Layer

M

MRI	Magnetic Resonance Imaging

N

Na_2HPO_4	Sodium phosphate dibasic
NaH_2	Sodium phosphate monobasic
NP	Nanoparticle
$NaHCO_3$	Sodium Bicarbonate
Na_2CO_3	Sodium Carbonate
NaCl	Sodium Chloride

P

PLGA	Poly(lactide-co-glycolide)
PTX	Paclitaxel
PBS	Phosphate Buffered Saline
PDI	Polydispersity Index
PDEGMA	Poly (di(ethylene glycol) methyl ether methacrylate
PLL	Poly-L-Lysine
PD-1	Programmed Cell Death 1
PD-L1	Programmed Cell Death Ligand 1

R

REDOX	Oxidation-reduction
RHAMM	Receptor for Hyaluronic acid-mediated motility
Rho	Rhodamine
RT	Radiotherapy
RNA	Ribonucleic Acid
rpm	Rotation per Minute

S

SEM	Scanning Electron Microscope
SERMs	Selective Estrogen Receptor Modulator
SPIONs	Superparamagnetic Iron Oxide Nanoparticle

T

TNBC	Triple Negative Breast Cancer
TME	Tumor Microenvironment

W

WHO	World Health Organization

"Enquanto não alcances
Não descanses.
De nenhum fruto queiras só metade."

Miguel Torga

Chapter 1.

General Information

CHAPTER 1- GENERAL INTRODUCTION

This first chapter presents the motivation behind the dissertation as well as an overview of breast cancer, typical treatments and current research for treatments.

1.1 MOTIVATION

Cancer is an uncontrolled growth of dysfunctional cells that can spread to other cells, organs and to other parts of the body. Benign tumors do not spread like malignant tumors, and usually do not require treatment or removal. Malignant tumors are treated by surgical removal, radio/chemotherapy, or combination of these. The treatment is often complicated due to development of metastases and multiple resistance, thus making cancer one of the deadliest diseases in modern societies [1].

According to *Dyba et al.*, there were approximately 2.7 million new cases of cancer in Europe in 2020. The different types of cancers that affect humans can be classified according to the affected anatomical part, the severity, and the metastatic potential. Four types of cancer represent about half (49.7%) of the overall burden: breast cancer (13.3%), colorectal cancer (12.7%), lung cancer (11.9%) and prostate cancer (12.5%) [2]. In 2020, according to *Sung et al.* there were 19.3 million new cases of cancer worldwide, where the most diagnosed type in both genders was breast cancer (11.7%), followed by lung cancer (11.4%), colorectal cancer (10%), prostate cancer (7.3%) and stomach cancer (5.6%) (**Figure 1.1**, **left**) [3].

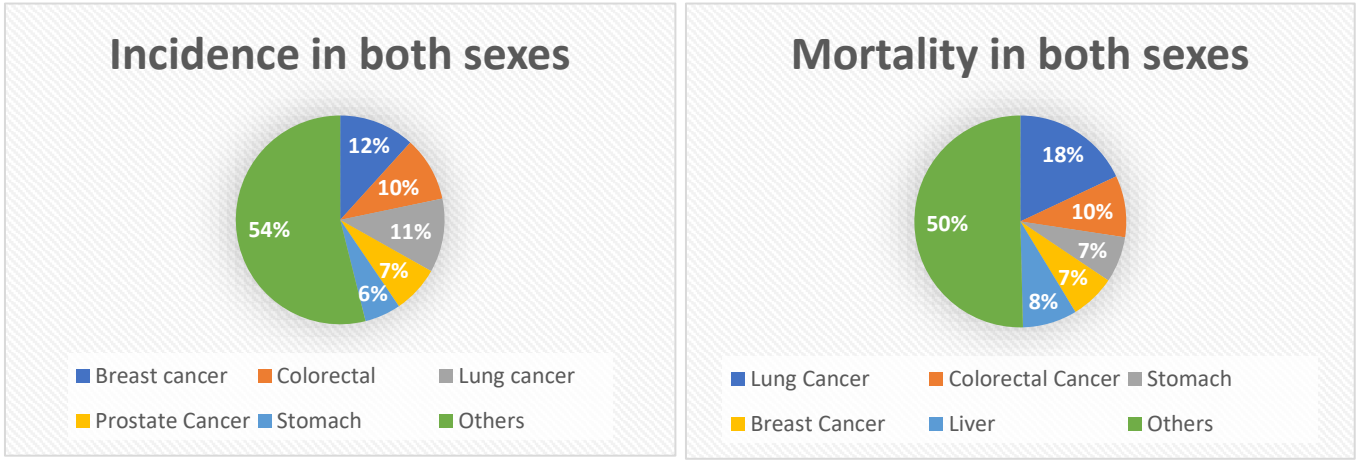

Figure 1. 1- Distribution of new cases and deaths in both sexes. Adapted from [3].

In women, the breast cancer was most prevalent (24.5%) (**Figure 2, left**) and in men this was the lung cancer (14.3%) (**Figure 1.2, right**). According to the same study, there were estimated 9.9 million deaths caused by cancer in 2020, with lung cancer classified as the deadliest (18%) followed by colorectal (9.4%), liver (8.3%), stomach (7.7%), and female breast cancer (6.9%) (**Figure 1.1, right**). In

women, breast cancer was also the most common cause of death (15.5%) (**Figure 1.3, left**), and in men the major cause of death continued to be lung cancer (21.5%) (**Figure 1.3, right**) [3].

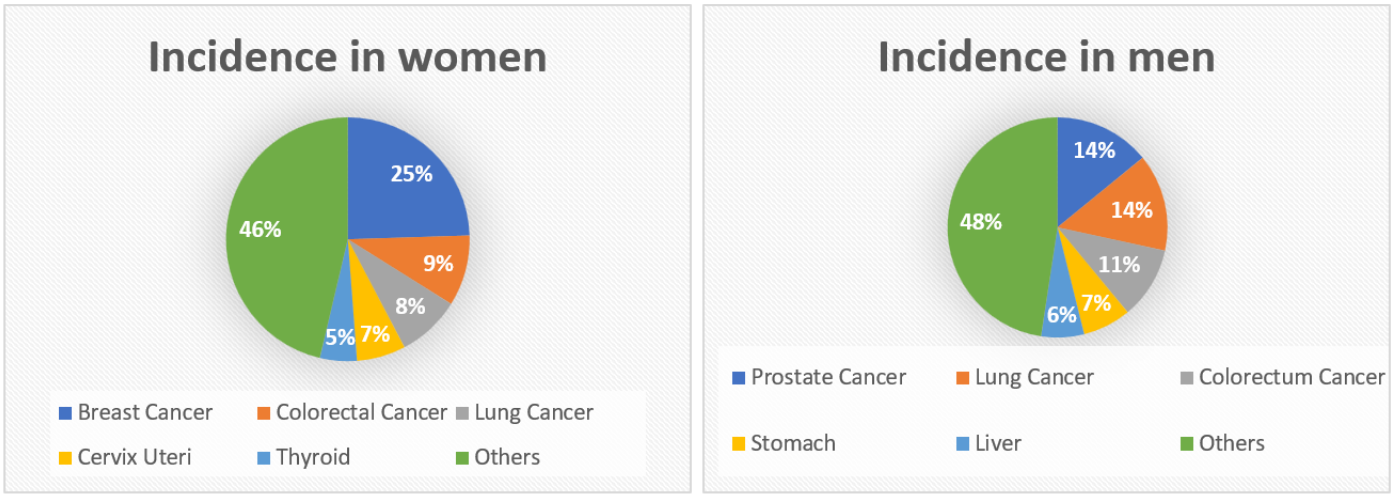

Figure 1. 2- Distribution of new cases in women and men. Adapted from [3].

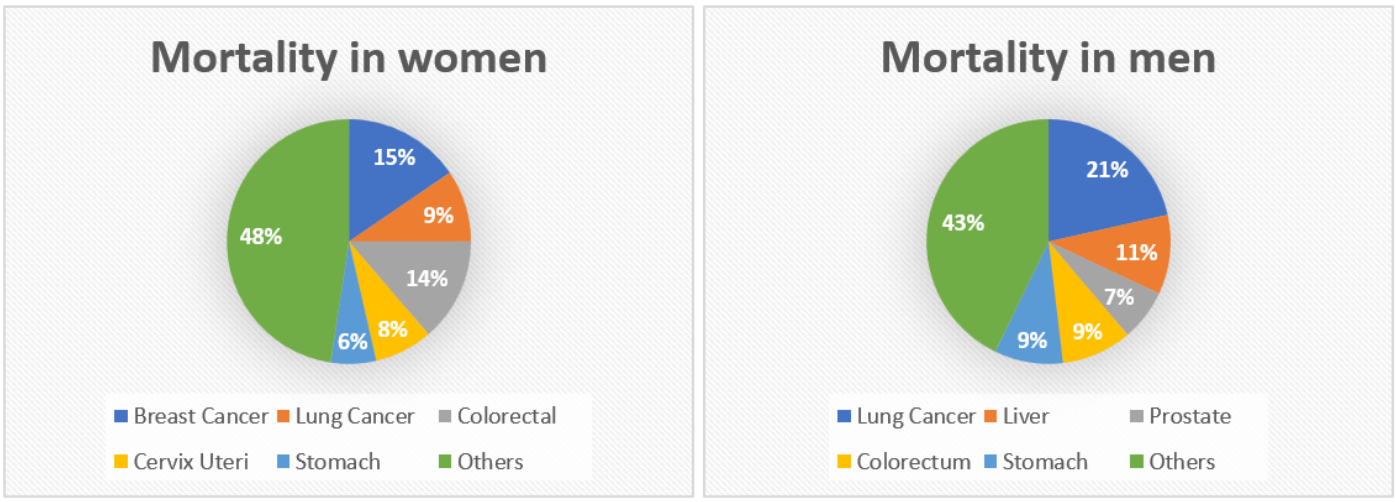

Figure 1. 3-Distribution of deaths in men and women. Adapted from [3].

Early detection and diagnosis decrease the mortality [4]. However, the symptoms are usually felt only when the tumor is already developed, i.e. it is difficult to diagnose cancer at an early stage when the available therapies are more efficient. The most common symptom is the growth of a mass or the process of ulceration. The current treatments for cancer are still limited: the effect of therapeutic agents depends on its targeted delivery through the hyperdeveloped extracellular matrix of tumor cells. A lot of effort has been put into targeting caveolin endocytic pathways [5], though due to the complex biochemistry of cancer, it is necessary to develop selective biomaterials/carriers that target multiple receptors that are overexpressed in cancer cells [6]. Therefore, in this study a drug delivery system that involves several bioactive components to endow targeting capacity against cancer cells and *in situ* release of anticancer drugs is proposed. Core/shell nanocapsules composed by calcium carbonate nanoparticles with capacity

for loading chemotherapeutics, and a layer-by-layer (LbL) coating comprising ligands for receptors that are overexpressed by the breast cancer cells will be developed.

1.2 BREAST CANCER

Breast cancer is highly heterogeneous and metastatic. An early diagnostic of this cancer is crucial not only to prevent tumor metastasis to different organs such as liver, lung, and brain, but also to increase the good prognosis and survival rate [4], [7]. The probability of developing breast cancer is related to some factors like gene mutation, estrogen levels, family history, lifestyle, aging, and gender. Routine exams by mammography and Magnetic Resonance Imaging (MRI) are the most common preventive practices and clinical means for diagnosis [4].

At molecular level, different types of breast cancer can be identified by immunohistochemistry using the hormone receptors (estrogen receptor (ER) and progesterone receptor (PR)), human epidermal growth factor receptor (HER2) and proliferation protein Ki-67 as markers [8], [9].Triple negative breast cancer (TNBC), as the name suggests, is characterized by the absence of ER, PR and HER2 overexpression and represents 15% of breast carcinomas [10]. TNBC is considered the most aggressive type of breast cancer, where the only treatment available is chemotherapy, because cells lack the typical biomarkers that can be targeted, i.e. current endocrine and anti-HER2 therapies are ineffective [11]. Luminal A breast cancer is ER and PR positive, HER2 negative and there is low expression of Ki-67 [9]. For this type of cancer, endocrine therapy is usually applied [12]. Luminal B breast cancer is ER positive, but there are two subtypes depending on HER2 status: for HER2 negative subtype (expression of PR is low or negative and expression of Ki-67 is high [9]), cytotoxic and endocrine therapies are recommended [12], while for HER2 positive subtype (no expression of PR and Ki-67) [9], anti-HER2 therapy is recommended along with a cytotoxic endocrine therapy [12]. Despite TNBC being the more invasive breast cancer, the cancer where ER expression is positive is the most common and the one responsible for most of the deaths [13].

1.3 CURRENT CLINICAL TREATMENTS

Table 1.1 gives an overview of the current clinical therapies as well as their advantages and disadvantages. The most common therapies are described in detail in the following subsections.

1.3.1 CHEMOTHERAPY

Chemotherapy is the most common treatment for breast cancer and the only treatment that provides an efficient therapeutic response in TNBC. It can be also applied in HR positive breast cancers but usually only at an advanced stage [14], [15].

There are different chemotherapeutics according to the cancer stage and the patient tolerance [16]. Anthracyclines, such as doxorubicin and epirubicin, are used to treat different types of cancer [17]. Doxorubicin has the capacity to intercalate inside DNA base pairs, thus inhibiting DNA and RNA synthesis and breaking DNA strands, causing an apoptosis [18].

For adjuvant chemotherapy (after surgery), an anthracycline-taxane therapy is recommended for patients who can tolerate it (usually for high-risk patients, i.e. with tumor that has size > 5 mm) [16]. Neoadjuvant chemotherapy (before surgery) is not common, but the use of carboplatin has shown some positive results in patients who received it. Nevertheless, this treatment is accompanied by a high toxicity [19].

The main cause of chemotherapy inefficiency is the development of drug resistance [20]. The problem is caused partly by a small population of cancer stem cells (CSC), capable of self-renewal, that can differentiate into cancer cells (**Figure 1.4**) [20]. CSCs are chemoresistant and after treatment their population is enriched and enter in a transient inactive status that could lead into metastasis or tumor recurrence [21]. This phenomenon is more concerning in TNBC since it is the type of breast cancer that has the most CSCs [16].

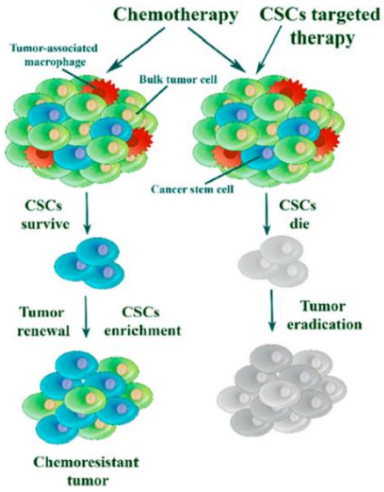

Figure 1. 4-Schematic presentation of the CSCs involvement in the development of drug resistance [16].

Secondary effects are the major drawback of chemotherapy: 79% of the patients with breast cancer suffer one side effect, 9% suffered one to three side effects, 5% experienced four to five and 7% six or more side effects. Side effects included chest pain, fatigue, constipation, diarrhea, pain, rash, mucositis, dyspnea, and vomiting [22].

1.3.2 RADIOTHERAPY

Radiotherapy (RT) is another approach used in 50% of all cancer patients. RT is commonly applied in combination with chemotherapy and/or surgery and aimed to reduce the risk of recurrence [23], [24]. Usually RT uses high-energy photons (6-25 MV) focused deep in the tissue while protect the skin from the radiation [23]. The major drawback of this therapy is the radiation effect over the healthy tissue [24]: RT is nonspecific, killing not only cancer cells but also healthy cells, and thus different side effects can be observed. Some studies have already proved that breast cancer patients are experiencing more severe psychosocial side effects than the patients with other cancers [25], and RT in breast cancer patients has been associated with an increase of heart diseases [24].

1.3.3 ENDOCRINE THERAPY

Endocrine therapy (ET) is used to treat luminal breast cancer. Using selective ER modulator (SERMs) or selective ER degraders (SERDs), ET can directly target the ER. It can also work with aromatase inhibitors by blocking estrogen synthesis in premenopausal patients with ovarian function suppression or postmenopausal patients, avoiding tumor cell replication and the activation of the ER pathway signaling [13]. Tissues that produce androgens, such as ovaries, adipose tissue, breast, and others, convert androgen into estrogen by aromatase. The ER dimerizes and translocate to the nucleus, after bond to estrogen, where ER dimers bind coactivators (CoA) to form a transcription active complex ER (**Figure 1.5A**) [26]. With SERMs, like tamoxifen, the binding of estrogen to ER are completely inhibit. SERM-bound ER dimers interact with the chromatin at estrogen response elements (ERE). Nevertheless, SERM-bound ER dimers are related with corepressors (CoR), that inhibit ER transcription in the breast (**Figure 1.5B**) [26]. Finally, with aromatase inhibitors the production of estrogen is blocked by the inhibition of aromatization of androgens to estrogens (**Figure 1.5C**) [26].

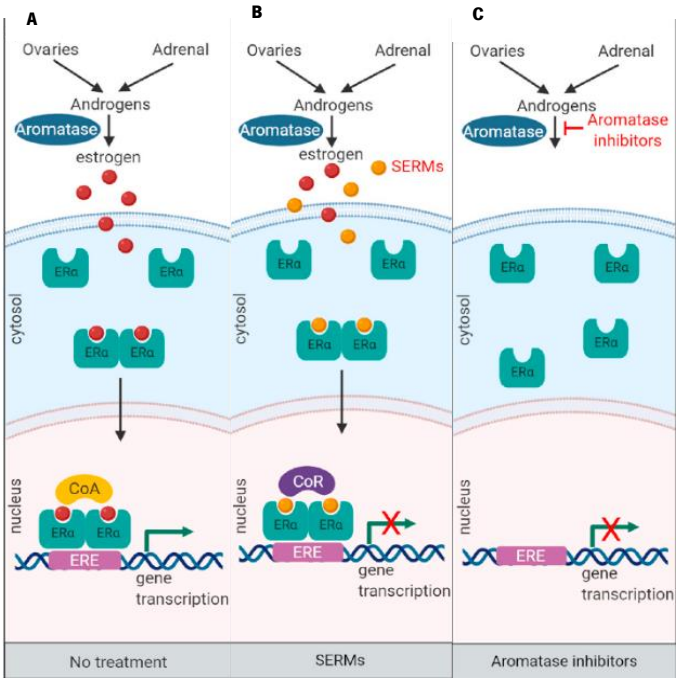

Figure 1. 5-Scheme of endocrine therapy. (A) Mechanism without treatment. (B) Mechanism of inhibition with SERMs. (C) Mechanism with aromatase inhibitors [26].

Tamoxifen is the most used agent for this therapy, over all stages of luminal breast cancer. Tamoxifen showed 53% of clinical benefit rate, a global response rate of 34% [13] and belongs to the list of essential drugs for the treatment of breast cancer issued by the World Health Organization (WHO). It is used not only to treat the cancer tissue but also to prevent recurrence after surgical removal of the tumor or in patients with high-risk to develop breast cancer. Aromatase inhibitors (AI) such as anastrozole, exemestane and letrozole are also used for ET [14]. Aromatase is the enzyme responsible for the synthesis of estrogens from androgenic substrates and AI suppress estrogen levels, inhibiting these enzyme [13]. AI are used for treatment of postmenopausal women, including women with ovarian suppression or when at least one ovary was removed [14].

1.3.4 ANTI-HER2 THERAPY

This therapy is applied for patients with luminal B breast cancer (HER2 positive). Different approaches have been developed to target HER2. These contain antibodies such as trastuzumab which targets domain IV of the receptor and pretuzumab which binds to domain II and inhibits the heterodimerization of HER2 with other ErbB receptor [27]. The first antibody used in clinics and approved by FDA, was the trastuzumab in combination with chemotherapy. Trastuzumab is a murine monoclonal antibody that targets HER2 [28]. Clinical studies demonstrated that this antibody increases the benefit of chemotherapy in luminal B breast cancer. A major side effect is cardiac dysfunction, observed mostly when a combinatory therapy of anthracycline and trastuzumab was applied [28].

It was recently shown that pertuzumab can increase the therapeutical efficacy when is combined with trastuzumab and chemotherapy [27]. Pertuzumab is a recombinant humanized monoclonal antibody, known as an inhibitor of heterodimerization of the HER2 receptors. It binds to a different HER2 epitope than trastuzumab [28]. However, when the patient develops resistance to trastuzumab, T-DM1 has been used as an alternative. This is an antibody-drug conjugate (ADC) that is toxic to cells overexpressing HER2 [27].

1.3.5 PD-1/PD-L1 INHIBITORS

Programmed cell death-1 (PD-1) is a regulatory protein located at the membrane surface of different immune cells, like natural killer T cells. Its ligand, PDL-1, is expressed at the cancer cell's surface [29]. Under normal conditions, the immune system has anti-cancer immune response that induces cancer cells apoptosis. However, tumor cells overexpress PD-L1, and thus PD-1/PDL-1 interactions inactivate T cells, failing the immune response against the tumor [30]–[32]. Current treatments involving the administration of PD-1/PD-L1 inhibitors are recommended especially in the late stage of TNBC [33]. PD-1/PDL-1 treatments mitigate the repression of the immune system and reactivate the T cell-mediated tumor cell death [31]. These inhibitors have shown efficacy not only in terms of tumor growth but also in terms of metastatic potential of breast cancers [29], [31]. However, antibodies therapies have some disadvantages related to the antibody's stability, immunogenicity, and production cost [34].

Table 1. 1-Common therapies for treatment of breast cancers and their main advantages and disadvantages.

Therapy	Advantages	Disadvantages
Chemotherapy	Best response from TNBC Can be applied before and after surgery	Kills healthy cells Inefficient against tumors with drug resistance Multiple side effects
Radiotherapy	Minimizes risk of cancer recurrence	Healthy tissue is exposed to radiation Increases the risk of developing heart diseases
Endocrine	Minimizes relapse after surgery removal on high-risk patients	Ineffective at advanced stages Efficacy rate of only 54%
Anti-HER2	Amplifies the outcome of chemotherapy	Can cause cardiac dysfunctions when combined with chemotherapy

PD-1/PD-L1 inhibitors	Efficient against advanced cancers	Low stability, low immunogenicity, and high production costs

1.4 EMERGING DESIGNS FOR ENHANCED DELIVERY SYSTEMS TARGETING CANCER

During the last decades, major efforts have been centered successively on the development of new drugs, whilst the efficacy of cancer treatments can be increased by lowering the damage of healthy tissues. Such effect can be achieved by either new drugs administered in free form or conventional drugs encapsulated in a matrix. Drug delivery systems have been shown to be more effective than drugs alone. In particular, nanoparticles have shown great promise across cancer research as discussed below.

1.4.1 NANOPARTICLES AS DRUG DELIVERY SYSTEMS

A drug delivery system (DDS) is described as a formulation or a device that facilitates the administration of a therapeutic agent into the body and enhances its efficacy and safety by managing the rate, timing, and location of drug release in the body [35]. In the last few years, the research of nanoparticles as drug delivery system has gained interest and developed into a wide variety of therapeutic uses [36]. In order to boost safety and effectiveness, NPs have the ability to improve the stability and solubility of encapsulated cargos, encourage movement across membranes, and increase circulation periods [37], [38]. Nanoparticles have been studied to overcome the limitations of several present medicines, showing high potential for drug delivery [39]. Table 1.2 summarizes the main types of nanoparticle systems that have been proposed as delivery systems for breast cancer treatment, which are described in more detail below.

Table 1. 2-Main types of NPs as drug delivery systems for breast cancer treatment.

Type of NPs	Cell line/animal model	Effect	Reference
FA-doxorubicin-IONP	MCF-7; BT549; MD-MBA-231 Female BALB/c nude mice	Strong cytotoxicity against breast cancer cells. Inhibition of tumor growth in mice model, while showing no toxicity against healthy organs	[44]

HA-SPIONs	MDA-MB-231; BALB/c female nude mice	Capacity to target MRI. Tumor cell suppression in vivo.	[45]
$SPION^{LA}$. $SPION^{LA\text{-}HAS}$; $SPION^{DEX}$	T-47D; BT-474; MCF7; MDA-MB-231; HUVEC as control	SPIONLA showed a cytotoxicity in control cells. SPIONDEX not suitable for drug delivery, but a potential candidate for MRI. SPIONLA-HAS are a good example for theragnostic applications.	[46]
PDEGMA	MDA-MB-231; HUVEC as control	NPs were easily internalized by cancer cells and inhibited tumor growth. Low toxicity to healthy cells.	[50]
Ch/γ-PGA	4T1	Developed a systemic therapeutic immune response against metastasizing mammary carcinoma	[51]
HCSL-NPs	4T1	Great tumor-targeting capacity, faster release of intracellular drugs, improvement of *in vitro* cytotoxicity against 4T1 cells	[52]

1.4.1.1. IRON OXIDE NANOPARTICLES

Iron Oxide Nanoparticles (IONPs) are the only magnetic nanoparticles approved by FDA for biomedical applications, and the only metal oxide approved for use in MRI. IONPs have high biocompatibility, low cost, and low toxicity [40], [41]. Usually, they are intravenously supplemented. This supplementation is the most effective way to reach targeted organs, though intratumoral or oral administrations (with lower doses of nanoparticles) are also possible [42]. Since IONPs can be used as MRI agents (*Diagnostics*) and as drug carriers (*Therapeutics*) a field called Theragnostics has emerged to contemplate strategies that incorporate this dual modality.

IONPs with 10 to 100 nm are considered superparamagnetic (and called SPIONs), i.e. they become magnetized rapidly when a magnetic field is applied, but not when the field is removed. As small are the IONP as fast and strong the response is [42]. This response enables guidance to a target place by employing an external magnet [35]. IONP can be modified to carry and release drugs in response to the tumor microenvironment (e.g. acidic pH) or to magnetic field [40] - when magnetized IONP vibrate and produce heat energy. This phenomenon is called hyperthermia and can be used alone or in combination with drugs [40]. When the result is high temperature (42°-46°C), cancer cells apoptosis is observed, while at lower temperatures, the susceptibility of cell to other treatments, e.g. chemotherapy, is enhanced [43].

In a study performed by *Pan et al.* [44], IONPs can be used with the pH-sensitive poly(β-thiopropionate) to produce nanoparticles with magnetic core and folic acid conjugation (FA-doxorubicin-IONPs) to target folate receptors overexpressed in breast cancer. This method has already demonstrated promising outcomes by inhibiting tumor development in female BALB/c nude mice (17±3 g, 4–5 weeks old) while being non-toxic to healthy organs. Additionally, MRI was effectively used to follow the accumulation of NP. These findings imply that theragnostic pH-sensitive nanoparticles may improve current cancer treatments [44].

In another design conducted by *Yang et al.* [45], IONPs have been modified with hyaluronic acid (HA), a glycosaminoglycan that targets CD44 receptors overexpressed in breast cancer cells. It revealed that by increasing the contrast in MRI, this method may be used for diagnostic purposes. Additionally, tumor cell suppression caused by photothermal activity was seen in *in vivo* experiments on BALB/c female nude mice (4-5 weeks, 18-20 g). Based on these findings, it was determined that HA-SPIONs offers high promise for cancer diagnosis and therapy [45].

In study by *Poller et al.* [46], three different types of SPIONs were evaluated in different cancer cells as well as in healthy cell as control. Lauric acid- coated SPIONs ($SPIONs^{LA}$), lauric acid- and human serum albumin-coated SPION ($SPIONs^{LA\text{-}HAS}$) and dextran-coated SPION ($SPIONs^{DEX}$). It was reported that the coating had strong effects in particle cellular internalization. Furthermore, it was shown that the uptake is dependent on cell type and that there are several forms of toxicity, which affects potential applications. Though $SPIONs^{LA}$ were found to be a good approach to target breast cancer cells, they showed cytotoxicity in healthy cells. $SPIONs^{DEX}$ demonstrated a high stability, ultra-low toxicity and hardly noticeable cell uptake, thus not being suitable for drug delivery, but could be a potential candidate for MRI. Based on $SPIONs^{LA\text{-}AS}$

magnetic characteristics, minimal toxicity and good stability, these type of SPIONs are more suitable for magnetic drug targeting but could also be used for MRI, allowing theragnostic applications [46].

1.4.1.2. POLYMERS NANOPARTICLES

Polymers can be used as building blocks of drug carriers with tailored structural, biochemical and biological activity. Synthetic polymers offer the advantage of strict control over their properties (e.g. charge, length, composition) but often lack bioactivity [47]. In contrast, natural biopolymers are usually highly heterogenous in terms of physicochemical properties that largely dependent on the source and extraction methods but are tailored by nature to perform highly specialized functions in their native niche [48].

Chitosan has been one of the most used biopolymers to develop drug carriers for anticancer agents due to its low cost, biodegradability and pH-responsiveness [49], [50]. However, chitosan often requires combination with other polymers to enhance encapsulation and delivery efficiency. For example, in a study performed by *Zhang et al.* [50], chitosan grafted with poly (di(ethylene glycol) methyl ether methacrylate) (PDEGMA) – a thermosensitive polymer – has been used to generate dual-responsive nanoparticles with high (i.e. above 70%) encapsulation efficiency. To enable specific internalization by breast cancer cells, this copolymer was further modified with HA. In this study, the anticancer drug utilized was paclitaxel (PTX), an FDA-approved drug that promotes cancer cells apoptosis. When it is used alone, PTX caused small tumor necrosis, but the healthy tissue was affected because of PTX accumulation and tumor resistance. With a targeted approach, HA-Ch-g-PDEGMA-PTX nanoparticles caused extensive apoptosis in tumor cells [50].

In another example by *Castro et al.* [51], radiotherapy was combined with chitosan/poly(γ-glutamic acid) nanoparticles (Ch/γ-PGA) to inhibit metastasis, increase immune response and control breast cancer progression. As mentioned before, the major difficulty in cancer therapy is the development of resistances against the drugs. In radiotherapy, which is based on inducing an immunogenic cell death, the presence of new antigens and release of death signals is stimulated, promoting the activation of immune system and recruitment of T cells to tumor site. This study demonstrated that these nanoparticles were capable of reprogramming macrophages with an immunosuppressive phenotype into an immunostimulatory one [51].

Li et al. [52] used histidine-grafted chitosan-lipoic acid NPs (HCSL-NPs) to evaluate their effectiveness of chemotherapy drug delivery for breast cancer treatment. These NPs, further supplemented with doxorubicin (DOX/HCSL-NPs), revealed good anticancer efficacy as well as less side effects *in vivo*. An improvement of *in vitro* cytotoxicity against 4T1 cells, increased internalization at extracellular pH, and faster release of intracellular drugs were observed. In BALB/c mice with breast cancer, great tumor-targeting capacity as well as high anticancer activity and low systemic toxicity was found. In conclusion, this strategy appears to offer great potential for the creation of drug delivery systems for the safe and effective treatment of breast cancer [52].

1.4.2 LAYER-BY-LAYER ASSEMBLY AND ITS IMPORTANCE IN TARGETING

A fundamental goal of cancer drug delivery is to selectively target cancer cells - and ideally not healthy cells. The overexpression of many cell surface receptors, including as integrins, folate receptors, and CD44 receptor, is important for surface targeting [53].

Zhou et al. [54], evaluated the selective cell targeting of folate receptors that are overexpressed in cancer cells [54], [55]. Poly(lactide-co-glycolide) PLGA nanoparticles were coated by LbL technique with biodegradable polyelectrolytes: alginate and chitosan. This pair was tested due to their presence of functional groups that can be applied to attach specialized recognition functions, such as folic acid. The approach provides an efficient method to coat NPs to minimize unspecific interaction and target receptors overexpressed in cancer cells [54].

In another study performed by *Suh et al.* [56], calcium phosphate nanoparticles coated with chitosan and hyaluronic acid were developed, to target CD44 receptors overexpressed in cancer cells. With an eight-fold improvement in therapeutic effectiveness above the medication alone, the targeting capacity of such nanoparticles was proven. The combination of active targeting of CD44 receptors with pH-sensitive nanoparticles allowed for target-specific drug delivery as well as increased anticancer medication efficacy, resulting in promising outcomes for cancer therapy [56].

Therefore, these findings show the possibility of employing LbL assembly in cancer drug delivery systems and the advantage of including hyaluronic acid in the coating as this polysaccharide is the major target of CD44 and receptor for hyaluronic acid-mediated motility (RHAMM) [57]–[59].

1.4.3 PRECISION ONCOLOGY

Precision oncology is a branch of precision medicine, an approach of treatment and prevention that considers individual variation of environment, genes, and lifestyle, focuses on oncological diseases [60]. Despite precision medicine is already applied during the practice of medicine, oncological diseases are the prime candidate for genomic treatment. It is important to understand the different mutations that occurs in cancers to administrate the adequate drug [61].

Recently, molecular therapeutic agents targeting specific actionable molecular modification were established with success, demonstrating that the use of molecular-based therapy to treat cancer is positive [62]. In a study conducted by *Sultova et al.* [63], it was discovered more than 30 mutations occurring in breast cancer, such as PIK3CA, ERBB2, KRAS and CCND1 mutations. Precision oncology is in constant evolution and different targets are being developed where different targets are being developed and respective therapies approved [63]. In 2019, FDA already approved Alpelisib, an oral α-specific PI3K inhibitor, to treat women with PIK3CA mutation, postmenopausal women with HR overexpressed and lack of amplification of HER2 and advanced or metastatic breast cancer followed with an endocrine therapy [64].

Although this therapy seems to be a good approach, the associated costs are still high for most patients. It is important to analyze the therapy cost-effectiveness in order to support their translation into clinical practice, e.g. establishing research programs and clinical trials [65].

1.5 PROPOSED STRATEGY FOR THE TREATMENT OF BREAST CANCER

The vast amount of therapies developed against cancer have been insufficient to lower the societal impact of this disease. The driving hypothesis of this project is that coating of drug-loaded nanoparticles with specific ECM-derived ligands will increase the internalization of chemotherapeutics by breast cancer cells. To this end, we will develop calcium carbonate ($CaCO_3$) nanoparticles as carriers for chemotherapeutic substances and coat them in a multilayered fashion with HA to target the CD44 receptors overexpressed in different aggressive breast cancers. This system could mitigate several problems of current cancer treatments, such as low encapsulation efficiency and off-targeted delivery. The latter is particularly important in cases of TNBC since the receptors targeted by conventional therapies are missing. A structure-activity relationship for this system will be established by assessment of the response of cancer cells with different aggressiveness.

1.5.1 CALCIUM CARBONATE PARTICLES

Nanoparticles concede stability to circulating drugs and thus improve their bioavailability and efficiency [66]. $CaCO_3$ is an inorganic material that shows pH-dependent dissolution, low toxicity, and slow biodegradability. $CaCO_3$ nanoparticles are easy to synthesize from commercially available and cheap reagents [67]. These nanoparticles are good candidates for tumor therapy due to their pH-sensitiveness: since the tumor microenvironment tends to be more acidic than normal tissue, these particles can dissolve in the cytoplasm and release the encapsulated agent(s) intracellularly [68]. There are three major anhydrous crystalline polymorphs of $CaCO_3$: calcite, vaterite and aragonite [69]. Under ambient temperature and pressure, rhomboidal calcite is the stable phase, while spherical-vaterite and needle-like aragonite are the metastable forms that easily convert into rhomboidal calcite [68], [69]. The reaction conditions, e.g. concentrations of the reagents, use of additives and temperature [68] can be adjusted to obtain different forms. Calcite is thermodynamically stable and has been combined with different polymers to develop sustained and targeted drug release systems for cancer treatment [70]. Aragonite is the densest phase of $CaCO_3$ and has been mostly used for bone repair [68], [71]. Vaterite is a good candidate for a controlled drug delivery system due to its larger pores, large surface area and quick decomposition under mild conditions [68], [70]. $CaCO_3$, can also be obtained in the amorphous state but it is typically unstable in aqueous environment, limiting its bioapplications [72]. Other limitation of amorphous $CaCO_3$ nanoparticles is their difficult synthesis that requires harsh conditions, such as high pressure, doping materials or other additives [73]. However, it has been shown that it is possible to synthesize a stable amorphous $CaCO_3$, for example, when it is doped due to electrostatics interactions, increasing the interest on these nanoparticles as a drug delivery system [74].

In previous studies, these nanoparticles have already shown promising results as a drug carrier for different types of cancer treatment. According to Kamba *et al.* [75], $CaCO_3$ nanocrystals loaded with doxorubicin demonstrated to be a good proposal as a delivery system for the treatment of osteosarcoma bone cancer, not only inhibiting MG 63 cell growth, but also showing faster release in an acidic environment (pH=4.8) than at physiological pH (7.4) [75].

In other study performed by Peng *et al.* [76], $CaCO_3$ nanospheres loaded with etoposide demonstrated to be more effective than free etoposide and $CaCO_3$. With etoposide loaded, they revealed to be cytotoxic against human gastric cancer cell line (SGC-7901) by suppressing tumor growth. Against normal cells, they showed 80% survival rate. Also, this pH-sensitive controlled release system released

80% of etoposide in acidic environment and about 30% at normal pH. These results suggested that it could be a promising approach to overpass the difficulties of current cancer treatments [76].

We intend to move forward with these nanoparticles to offer a selective therapy against breast cancer. Because the tumor microenvironment of breast cancer is more acidic than normal tissue and the reported results with these NPs demonstrated the pH-selectiveness, it is indicative of a promising proposal for drug delivery in distinct types of cancer.

1.5.2 LAYER-BY-LAYER

The primary goal of drug delivery systems is to deliver drugs at the proper concentration to the specific target site. The use of thin films in drug delivery has recently gained attention due to its capacity to properly load drugs and release them in a regulated way, which increases therapeutic effectiveness [77]. Techniques for creating ultrathin film devices include Langmuir–Blodgett method, self-assembled monolayer techniques and layer-by-layer (LbL) assembly [78].

Due to the lack of limits on the size or form of the substrate and the absence of high temperatures or pressure, LbL assembly is ideal for the creation of films used for drug delivery. The LbL assembly procedure involves the alternate adsorption of the interacting components, which results in the deposition of multilayer films onto the substrate's surface [79]. Its composition can be strikingly versatile: virtually any charged material can be used as a building in LbL, from inorganic particles to bioactive polymers, and these can adsorb to a chosen substrate of any shape [80]–[82]. The assembly procedure is tipically based on the alternate immersion of the substrate in polyelectrolyte solutions of opposite charge (**Figure 1.6**). While electrostatic interactions are commonly used to drive LbL assembly – using polyelectrolytes as building blocks – other interactions have been explored, such as hydrophobic interactions, hydrogen bonding, coordination chemistry, stereo complexation, among others [80], [83]. Depending on the materials employed in the specific multilayer film carrying the drug, these features enable the regulated release of the drug. As a result, the LbL process may be regarded as the best technique for creating nano-multilayer films containing therapeutic compounds [77].

Some examples of polyelectrolytes used in LbL are the cationic poly-L-lysine (PLL) and the anionic HA. These materials have been selected to conduct this project based on their properties. PLL is a cationic polypeptide thanks to the presence of amino groups in its structure. It is commonly used in promoting cell adhesion to solid substrates, and the attachment of bioactive molecules [84], thus assuming not a bioactive role but a structural one. HA is a linear glycosaminoglycan composed of one *N*-acetylated

glucosamine and one glucuronic acid. The latter presents the carboxyl groups that render HA negatively charged and has a pK_a of around 3.5 [85]. As previously mentioned, HA is indispensable to target the overexpressed CD44 receptors by establishing monovalent bonds with CD44, thus avoiding receptor clustering [86], [87]. Despite CD44 being the primary binding receptor for HA, that bonding depends on the type of cell involved since the expression of CD44 may vary according to the aggressiveness and metastatic potential of the cells[88]. Because of that, CD44 can be used to discriminate between normal and cancer tissues in a targeted therapy [89]. PLL will be intercalated with HA to construct films with variable number of layers, and thus tunable thickness and HA targeting ability.

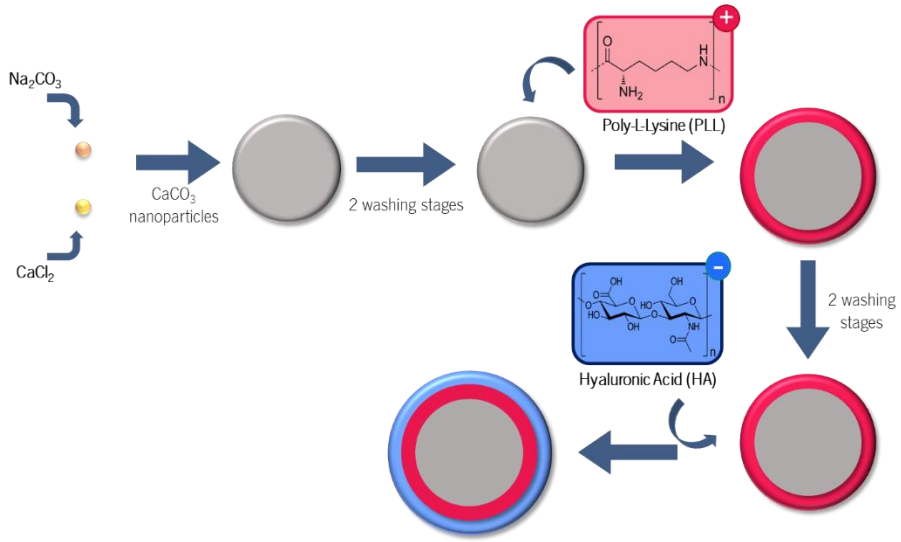

Figure 1. 6- Scheme of layer-by-layer assembly.

1.6 REFERENCES

[1] J.-J. Wang, K.-F. Lei, and F. Han, "Tumor microenvironment: recent advances in various cancer treatments," *Eur Rev Med Pharmacol Sci*, vol. 22.12, pp. 3855–3864, 2018.

[2] T. Dyba *et al.*, "ScienceDirect The European cancer burden in 2020 : Incidence and mortality estimates for 40 countries and 25 major cancers," vol. 157, 2021.

[3] H. Sung *et al.*, "Global Cancer Statistics 2020: GLOBOCAN Estimates of Incidence and Mortality Worldwide for 36 Cancers in 185 Countries," *CA. Cancer J. Clin.*, vol. 71, no. 3, pp. 209–249, 2021.

[4] Y. S. Sun *et al.*, "Risk factors and preventions of breast cancer," *International Journal of Biological Sciences*, vol. 13, no. 11. Ivyspring International Publisher, pp. 1387–1397, 2017.

[5] U. E. Martinez-Outschoorn, F. Sotgia, and M. P. Lisanti, "Caveolae and signalling in cancer," *Nature Reviews Cancer*, vol. 15, no. 4. Nature Publishing Group, pp. 225–237, 2015.

[6] S. A. Dugger, A. Platt, and D. B. Goldstein, "Drug development in the era of precision medicine," *Nature Reviews Drug Discovery*, vol. 17, no. 3. Nature Publishing Group, pp. 183–196, 2018.

[7] M. Razzak and L. Marshall, "Breast Cancer Primeview," *Nat. Rev. Dis. Prim.*, 2019.

[8] S. Loibl, P. Poortmans, M. Morrow, C. Denkert, and G. Curigliano, "Breast cancer," *The Lancet*, vol. 397, no. 10286. Elsevier B.V., pp. 1750–1769, 2021.

[9] R. Erber and A. Hartmann, "Histology of Luminal Breast Cancer," *Breast Care*, vol. 15, no. 4. S. Karger AG, pp. 327–336, 2020.

[10] P. Kumar and R. Aggarwal, "An overview of triple-negative breast cancer," *Archives of Gynecology and Obstetrics*, vol. 293, no. 2. Springer Verlag, pp. 247–269, 2016.

[11] C. Denkert, C. Liedtke, A. Tutt, and G. von Minckwitz, "Molecular alterations in triple-negative breast cancer—the road to new treatment strategies," *The Lancet*, vol. 389, no. 10087. Lancet Publishing Group, pp. 2430–2442, 2017.

[12] H. B. Luo *et al.*, "Differentiation between Luminal A and B Molecular Subtypes of Breast Cancer Using Pharmacokinetic Quantitative Parameters with Histogram and Texture Features on Preoperative Dynamic Contrast-Enhanced Magnetic Resonance Imaging," *Acad. Radiol.*, vol. 27, no. 3, pp. e35–e44, 2020.

[13] T. Reinert, B. de Paula, M. N. Shafaee, P. H. Souza, M. J. Ellis, and J. Bines, "Endocrine therapy for ER-positive/HER2-negative metastatic breast cancer," *Chinese Clin. Oncol.*, vol. 7, no. 3, 2018.

[14] A. G. Waks and E. P. Winer, "Breast Cancer Treatment: A Review," *JAMA - Journal of the American Medical Association*, vol. 321, no. 3. American Medical Association, pp. 288–300, 2019.

[15] L. N. Chaudhary, K. H. Wilkinson, and A. Kong, "Triple-Negative Breast Cancer: Who Should Receive Neoadjuvant Chemotherapy?," *Surgical Oncology Clinics of North America*, vol. 27, no. 1. W.B. Saunders, pp. 141–153, 2018.

[16] M. Nedeljković and A. Damjanović, "Mechanisms of Chemotherapy Resistance in Triple-Negative

Breast Cancer-How We Can Rise to the Challenge," *Cells*, vol. 8, no. 9. NLM (Medline), 2019.

[17] M. Khasraw, R. Bell, and C. Dang, "Epirubicin: Is it like doxorubicin in breast cancer? A clinical review," *Breast*, vol. 21, no. 2. Churchill Livingstone, pp. 142–149, 2012.

[18] K. Johnson-Arbor and R. Dubey, *Doxorubicin*. StatPearls Publishing LLC, 2021.

[19] J. M. Lebert, R. Lester, E. Powell, M. Seal, and J. McCarthy, "Advances in the systemic treatment of triple-negative breast cancer," *Current Oncology*, vol. 25. Multimed Inc., pp. S142–S150, 2018.

[20] H. E. Lee *et al.*, "An increase in cancer stem cell population after primary systemic therapy is a poor prognostic factor in breast cancer," *Br. J. Cancer*, vol. 104, no. 11, pp. 1730–1738, 2011.

[21] M. Shibata and M. O. Hoque, "Targeting cancer stem cells: A strategy for effective eradication of cancer," *Cancers*, vol. 11, no. 5. MDPI AG, 2019.

[22] A. Pearce *et al.*, "Incidence and severity of self-reported chemotherapy side effects in routine care: A prospective cohort study," *PLoS One*, vol. 12, no. 10, 2017.

[23] C. Allen, S. Her, and D. A. Jaffray, "Radiotherapy for Cancer: Present and Future," *Advanced Drug Delivery Reviews*, vol. 109. Elsevier B.V., pp. 1–2, 2017.

[24] C. W. Taylor and A. M. Kirby, "Cardiac Side-effects From Breast Cancer Radiotherapy," *Clin. Oncol.*, vol. 27, no. 11, pp. 621–629, 2015.

[25] P. A. Williams, S. Cao, D. Yang, and R. L. Jennelle, "Patient-reported outcomes of the relative severity of side effects from cancer radiotherapy," *Support. Care Cancer*, vol. 28, no. 1, pp. 309–316, 2020.

[26] A. B. Hanker, D. R. Sudhan, and C. L. Arteaga, "Overcoming Endocrine Resistance in Breast Cancer," *Cancer Cell*, vol. 37, no. 4. Cell Press, pp. 496–513, 2020.

[27] A. Ocaña, E. Amir, and A. Pandiella, "HER2 heterogeneity and resistance to anti-HER2 antibody-drug conjugates," *Breast Cancer Research*, vol. 22, no. 1. BioMed Central Ltd., 2020.

[28] M. Yao and P. Fu, "Advances in anti-HER2 therapy in metastatic breast cancer," *Chinese Clinical Oncology*, vol. 7, no. 3. AME Publishing Company, 2018.

[29] A. Monneur, A. Gonçalves, and F. Bertucci, "Expression de PD-L1 et inhibiteurs de la voie PD-

1/PD-L1 dans le cancer du sein," *Bulletin du Cancer*, vol. 105, no. 3. John Libbey Eurotext, pp. 263–274, 2018.

[30] K. Li and H. Tian, "Development of small-molecule immune checkpoint inhibitors of PD-1/PD-L1 as a new therapeutic strategy for tumour immunotherapy," *Journal of Drug Targeting*, vol. 27, no. 3. Taylor and Francis Ltd, pp. 244–256, Mar. 16, 2019.

[31] L. Ai *et al.*, "Research status and outlook of pd-1/pd-l1 inhibitors for cancer therapy," *Drug Design, Development and Therapy*, vol. 14. Dove Medical Press Ltd, pp. 3625–3649, 2020.

[32] C. Caldwell, C. E. Johnson, V. N. Balaji, G. A. Balaji, R. D. Hammer, and R. Kannan, "Identification and Validation of a PD-L1 Binding Peptide for Determination of PDL1 Expression in Tumors," *Sci. Rep.*, vol. 7, no. 1, 2017.

[33] W. Zou, J. D. Wolchok, and L. Chen, "PD-L1 (B7-H1) and PD-1 pathway blockade for cancer therapy: Mechanisms, response biomarkers, and combinations," *Sci. Transl. Med.*, vol. 8, no. 328, 2016.

[34] E. A. Mittendorf *et al.*, "PD-L1 expression in triple-negative breast cancer," *Cancer Immunol. Res.*, vol. 2, no. 4, pp. 361–370, 2014.

[35] I. C. Lee, Y. C. Wu, E. M. Cheng, and W. T. Yang, "Biomimetic niche for neural stem cell differentiation using poly-L-lysine/hyaluronic acid multilayer films," *J. Biomater. Appl.*, vol. 29, no. 10, pp. 1418–1427, 2015.

[36] M. J. Mitchell, M. M. Billingsley, R. M. Haley, R. Langer, M. E. Wechsler, and N. A. Peppas, "Engineering precision nanoparticles," *Nat. Rev. Drug Discov.*, 2021.

[37] E. Blanco, H. Shen, and M. Ferrari, "HHS Public Access," vol. 33, no. 9, pp. 941–951, 2016.

[38] L. Kou, Y. D. Bhutia, Q. Yao, Z. He, and J. Sun, "Transporter-Guided Delivery of Nanoparticles to Improve Drug Permeation across Cellular Barriers and Drug Exposure to Selective Cell Types Effects from Conventional Properties," vol. 9, no. January, pp. 1–16, 2018.

[39] S. Mitragotri *et al.*, "Drug Delivery Research for the Future : Expanding the Nano Horizons and Beyond," *J. Control. Release*, vol. 246, pp. 183–184, 2017.

[40] S. Thoidingjam and A. B. Tiku, "New developments in breast cancer therapy: Role of iron oxide nanoparticles," *Advances in Natural Sciences: Nanoscience and Nanotechnology*, vol. 8, no. 2.

IOP Publishing Ltd, 2017.

[41] P. Martinkova, M. Brtnicky, J. Kynicky, and M. Pohanka, "Iron Oxide Nanoparticles: Innovative Tool in Cancer Diagnosis and Therapy," *Advanced Healthcare Materials*, vol. 7, no. 5. Wiley-VCH Verlag, 2018.

[42] Wahajuddin and S. Arora, "Superparamagnetic iron oxide nanoparticles: Magnetic nanoplatforms as drug carriers," *International Journal of Nanomedicine*, vol. 7. pp. 3445–3471, 2012.

[43] S. Talluri and R. R. Malla, "Superparamagnetic Iron Oxide Nanoparticles (SPIONs) for Diagnosis and Treatment of Breast, Ovarian and Cervical Cancers," *Curr. Drug Metab.*, vol. 20, no. 12, pp. 942–945, 2019.

[44] C. Pan *et al.*, "Theranostic ph-sensitive nanoparticles for highly efficient targeted delivery of doxorubicin for breast tumor treatment," *Int. J. Nanomedicine*, vol. 13, pp. 1119–1137, 2018, [Online]. Available: http://dx.doi.org/10.2147/IJN.S147464.

[45] R. M. Yang *et al.*, "Hyaluronan-modified superparamagnetic iron oxide nanoparticles for bimodal breast cancer imaging and photothermal therapy," *Int. J. Nanomedicine*, vol. 12, pp. 197–206, 2017.

[46] J. M. Poller *et al.*, "Selection of potential iron oxide nanoparticles for breast cancer treatment based on in vitro cytotoxicity and cellular uptake," *Int. J. Nanomedicine*, vol. 12, pp. 3207–3220, 2017.

[47] L. J. Fetters,', + D J Lohse, D. Richter, T. A. Witten, and A. Zirkelt, "Connection between Polymer Molecular Weight, Density, Chain Dimensions, and Melt Viscoelastic Properties," 1994.

[48] M. A. Meyers, P. Y. Chen, A. Y. M. Lin, and Y. Seki, "Biological materials: Structure and mechanical properties," *Progress in Materials Science*, vol. 53, no. 1. pp. 1–206, 2008.

[49] Y. Herdiana, N. Wathoni, S. Shamsuddin, I. M. Joni, and M. Muchtaridi, "Chitosan-based nanoparticles of targeted drug delivery system in breast cancer treatment," *Polymers*, vol. 13, no. 11. MDPI AG, 2021.

[50] X. Zhang *et al.*, "Dual-responsive nanoparticles based on chitosan for enhanced breast cancer therapy," *Carbohydr. Polym.*, vol. 221, pp. 84–93, 2019.

[51] F. Castro *et al.*, "Chitosan/γ-PGA nanoparticles-based immunotherapy as adjuvant to radiotherapy in breast cancer," *Biomaterials*, vol. 257, 2020.

[52] F. Castro *et al.*, "Pro-inflammatory chitosan/poly(γ-glutamic acid) nanoparticles modulate human antigen-presenting cells phenotype and revert their pro-invasive capacity," *Acta Biomater.*, vol. 63, pp. 96–109, 2017.

[53] X. Q. Liu and C. Picart, "Layer-by-Layer Assemblies for Cancer Treatment and Diagnosis," *Adv. Mater.*, vol. 28, no. 6, pp. 1295–1301, 2016.

[54] J. Zhou, G. Romero, E. Rojas, L. Ma, S. Moya, and C. Gao, "Layer by layer chitosan/alginate coatings on poly(lactide-co-glycolide) nanoparticles for antifouling protection and Folic acid binding to achieve selective cell targeting," *J. Colloid Interface Sci.*, vol. 345, no. 2, pp. 241–247, 2010.

[55] H. Zhao and L. Y. L. Yung, "Selectivity of folate conjugated polymer micelles against different tumor cells," *Int. J. Pharm.*, vol. 349, no. 1–2, pp. 256–268, 2008.

[56] M. S. Suh, J. Shen, L. T. Kuhn, and D. J. Burgess, "Layer-by-layer nanoparticle platform for cancer active targeting," *Int. J. Pharm.*, vol. 517, no. 1–2, pp. 58–66, 2017.

[57] A. M. Carvalho, D. Soares da Costa, P. M. R. Paulo, R. L. Reis, and I. Pashkuleva, "Co-localization and crosstalk between CD44 and RHAMM depend on hyaluronan presentation," *Acta Biomater.*, vol. 119, pp. 114–124, 2021.

[58] A. M. Carvalho, D. Soares da Costa, R. L. Reis, and I. Pashkuleva, "RHAMM expression tunes the response of breast cancer cell lines to hyaluronan," *Acta Biomater.*, vol. 146, pp. 187–196, 2022.

[59] A. M. Carvalho, D. Soares da Costa, R. L. Reis, and I. Pashkuleva, "Influence of Hyaluronan Density on the Behavior of Breast Cancer Cells with Different CD44 Expression," *Adv. Healthc. Mater.*, vol. 11, no. 4, pp. 1–9, 2022.

[60] Y. Naito and T. Urasaki, "Precision medicine in breast cancer," *Chinese Clinical Oncology*, vol. 7, no. 3. AME Publishing Company, 2018.

[61] E. Liow and B. Tran, "Precision oncology in urothelial cancer," *ESMO Open*, vol. 5. BMJ Publishing Group, 2020.

[62] D. S. Haslem *et al.*, "Precision oncology in advanced cancer patients improves overall survival with lower weekly healthcare costs," 2018.

[63] E. Sultova *et al.*, "NGS-guided precision oncology in metastatic breast and gynecological cancer: first experiences at the CCC Munich LMU," *Arch. Gynecol. Obstet.*, vol. 303, no. 5, pp. 1331–1345, 2021.

[64] D. Y. Chang, W. L. Ma, and Y. S. Lu, "Role of alpelisib in the treatment of pik3ca-mutated breast cancer: Patient selection and clinical perspectives," *Ther. Clin. Risk Manag.*, vol. 17, pp. 193–207, 2021.

[65] A. Rody, J. Ettl, F. Marmé, and A. Prat, "Molecular Tumor Boards," *Breast Care*, vol. 13, no. 2. S. Karger AG, pp. 141–143, 2018.

[66] P. Fadia *et al.*, "Calcium carbonate nano- and microparticles: synthesis methods and biological applications," *3 Biotech*, vol. 11, no. 11. Springer Science and Business Media Deutschland GmbH, 2021.

[67] V. Popova, Y. Poletaeva, I. Pyshnaya, D. Pyshnyi, and E. Dmitrienko, "Designing pH-dependent systems based on nanoscale calcium carbonate for the delivery of an antitumor drug," *Nanomaterials*, vol. 11, no. 11, 2021.

[68] S. Maleki Dizaj, M. Barzegar-Jalali, M. H. Zarrintan, K. Adibkia, and F. Lotfipour, "Calcium carbonate nanoparticles as cancer drug delivery system," *Expert Opinion on Drug Delivery*, vol. 12, no. 10. Taylor and Francis Ltd, pp. 1649–1660, 2015.

[69] Y. Svenskaya *et al.*, "Anticancer drug delivery system based on calcium carbonate particles loaded with a photosensitizer," *Biophys. Chem.*, vol. 182, pp. 11–15, 2013.

[70] S. Maleki Dizaj, S. Sharifi, E. Ahmadian, A. Eftekhari, K. Adibkia, and F. Lotfipour, "An update on calcium carbonate nanoparticles as cancer drug/gene delivery system," *Expert Opinion on Drug Delivery*, vol. 16, no. 4. Taylor and Francis Ltd, pp. 331–345, 2019.

[71] K. N. Islam *et al.*, "Facile synthesis of calcium carbonate nanoparticles from cockle shells," *J. Nanomater.*, vol. 2012, 2012.

[72] C. F. Dai, W. Y. Wang, L. Wang, L. Zhou, S. P. Li, and X. D. Li, "Synthesis of nanostructured calcium carbonate/methotrexate@silica and its application in cancer therapy," *RSC Adv.*, vol. 6,

no. 72, pp. 68335–68340, 2016.

[73] Avik Som *et al.*, "Monodispersed calcium carbonate nanoparticles modulate local pH and inhibit tumor growth in vivo," in *Nanoscale*, 2017, vol. 2019-November.

[74] Y. Ueno, H. Futagawa, Y. Takagi, A. Ueno, and Y. Mizushima, "Drug-incorporating calcium carbonate nanoparticles for a new delivery system," *J. Control. Release*, vol. 103, no. 1, pp. 93–98, 2005.

[75] S. A. Kamba, M. Ismail, S. H. Hussein-Al-Ali, T. A. T. Ibrahim, and Z. A. B. Zakaria, "In vitro delivery and controlled release of doxorubicin for targeting osteosarcoma bone cancer," *Molecules*, vol. 18, no. 9, pp. 10580–10598, 2013.

[76] H. Peng *et al.*, "Preparation of hierarchical mesoporous CaCO3 by a facile binary solvent approach as anticancer drug carrier for etoposide," *Nanoscale Res. Lett.*, vol. 8, no. 1, pp. 1–11, 2013.

[77] S. Park, U. Han, D. Choi, and J. Hong, "Layer-by-layer assembled polymeric thin films as prospective drug delivery carriers: Design and applications," *Biomater. Res.*, vol. 22, pp. 1–13, 2018.

[78] M. H. Park, S. S. Agasti, B. Creran, C. Kim, and V. M. Rotello, "Controlled and sustained release of drugs from dendrimer-nanoparticle composite films," *Adv. Mater.*, vol. 23, no. 25, pp. 2839–2842, 2011.

[79] K. Ariga, Y. M. Lvov, K. Kawakami, Q. Ji, and J. P. Hill, "Layer-by-layer self-assembled shells for drug delivery," *Adv. Drug Deliv. Rev.*, vol. 63, no. 9, pp. 762–771, 2011.

[80] I. S. Elizarova and P. F. Luckham, "Layer-by-layer adsorption: Factors affecting the choice of substrates and polymers," *Advances in Colloid and Interface Science*, vol. 262. Elsevier B.V., pp. 1–20, 2018.

[81] J. Borges and J. F. Mano, "Molecular interactions driving the layer-by-layer assembly of multilayers," *Chemical Reviews*, vol. 114, no. 18. American Chemical Society, pp. 8883–8942, 2014.

[82] R. R. Costa and J. F. Mano, "Polyelectrolyte multilayered assemblies in biomedical technologies," *Chemical Society Reviews*, vol. 43, no. 10. Royal Society of Chemistry, pp.

3453–3479, 2014.

[83] Katsuhiko SATO, Shigehiro TAKAHASHI, and Jun-ichi ANZAI, "Layer-by-layer Thin Films and Microcapsules for Biosensors and Microcapsules for Biosensors andControlled Release," *Japan Soc. Anal. Chem.*, vol. 28, pp. 929–938, 2012.

[84] F. Kuralay, N. Dükar, and Y. Bayramlı, "Poly-L-lysine Coated Surfaces for Ultrasensitive Nucleic Acid Detection," *Electroanalysis*, vol. 30, no. 7, pp. 1556–1565, 2018.

[85] J. Seog, D. Dean, A. H. K. Plaas, S. Wong-Palms, A. J. Grodzinsky, and C. Ortiz, "Direct measurement of glycosaminoglycan intermolecular interactions via high-resolution force spectroscopy," *Macromolecules*, vol. 35, no. 14, pp. 5601–5615, 2002.

[86] S. Misra *et al.*, "Hyaluronan-CD44 interactions as potential targets for cancer therapy," *FEBS Journal*, vol. 278, no. 9. pp. 1429–1443, 2011.

[87] R. Thapa and G. D. Wilson, "The Importance of CD44 as a Stem Cell Biomarker and Therapeutic Target in Cancer," *Stem Cells International*, vol. 2016. Hindawi Limited, 2016.

[88] P. W. Noble *et al.*, "The structure and regulation of hyaluronan-binding proteins," 1999.

[89] G. Mattheolabakis, L. Milane, A. Singh, and M. M. Amiji, "Hyaluronic acid targeting of CD44 for cancer therapy: From receptor biology to nanomedicine," *J. Drug Target.*, vol. 23, no. 7–8, pp. 605–618, 2015.

CHAPTER 2.

MATERIALS AND METHODS

CHAPTER 2- MATERIALS AND METHODS

This section describes the materials and procedures used to get the experimental results provided in this dissertation. Additionally, a description of the characterization techniques utilized is included.

2.1. MATERIALS

2.1.1. HYALURONIC ACID

Sodium hyaluronate was purchased from Lifecore (ref. HA20K-5, molecular weight 21-40KDa).

As shown in **Figure 2.1**, Hyaluronic Acid (HA) is an anionic biopolymer is made up of repeating disaccharide units of β(1,4)-D-glucuronic acid and β(1,3)-N-acetyl-D-glucosamine [1], [2]. This natural biopolymer's architecture has good physicochemical characteristics including biocompatibility, non-toxicity, non-immunogenicity, non-inflammatory, and entirely biodegradable properties [3]. HA may be employed in a variety of sectors, with oncology being one that potentially sees more wide applications. The amount of body receptors with a specific affinity for HA that may be targeted, such as RHAMM (receptor for hyaluronic-mediated motility) and CD44, is connected with its capacity for drug delivery [3]–[6]. In comparison to other polysaccharides, this places HA in the forefront of cancer-related drug delivery research [7].

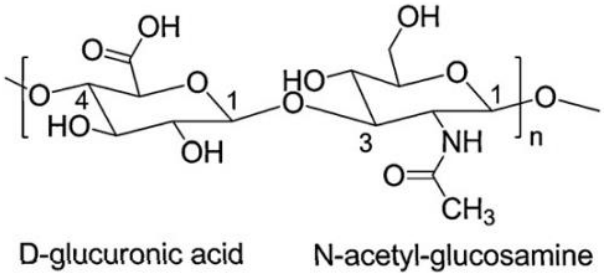

Figure 2. 1-Chemical structure of hyaluronic acid [1].

2.1.2. POLY-L-LYSINE

Poly-L-lysine hydrobromide was purchased from Laborspirit (ref. P7890-500MG, molecular weight 15-30kDa by viscosity).

Poly-L-Lysine (PLL) is a cationic biopolymer that dissolves in water and contains the monomer α-L-lysine (**Figure 2.2**) [8]. It has received special interest for a variety of biological and pharmaceutical applications due to its inherent non-antigenicity, antibacterial activity, biocompatibility, and biodegradability [9]. Because of the ability of PLL to interact with anionic

polymers via electrostatic interactions, it has been widely applied to produce polyelectrolyte multilayers by sequentially depositing oppositely charged polymers onto a solid surface [10]–[12]. It has been shown that layer-by-layer technique of HA and PL is a viable method for developing biomaterials that can mimic the native extracellular matrix and regulate drug release [13].

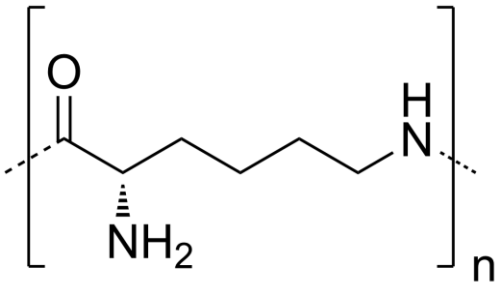

Figure 2. 2-Chemical structure of poly-L-lysine [13].

2.1.3. ETHYLENE GLYCOL

Ethylene Glycol was purchased from ChemicalNor (ref. 102466).

Ethylene glycol (EG) -**Figure 2.3**- is an odorless and colorless organic solvent that has been used in the natural gas business as a drying agent, in cooling and heating systems as an antifreeze, and in the textile, plastic, and paint industries. Furthermore, EG has been utilized in the production of shape-controlled particles [14], [15]. This phenomenon in nanoparticles has gained interest, especially in calcium carbonate ($CaCO_3$) synthesis by offering a decreased solubility and increased density [16]. Some studies have already reported that particle size is lowered by increasing EG concentration. Also, the impact of EG on the transition time of nanoparticles is induced by the solvent itself, most likely as a result of kinetic stabilization by slowing the growth rate of the more stable $CaCO_3$ [17], [18].

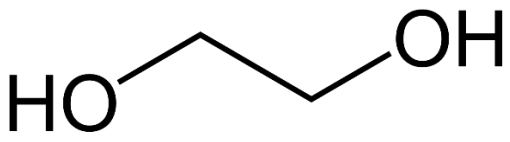

Figure 2. 3- Chemical structure of Ethylene Glycol [15].

2.1.4. HEPARIN

Heparin sodium salt from porcine intestinal mucosa was purchased from Laborspirit (ref. H3393, Grade I-A, ≥180 USP units/mg).

Heparin (**Figure 2.4**) is a linear polysaccharide made up of repeated units of 2-amino2-deoxyglucopyranose (D-glucosamine, GlcN) and 1-4 linked pyranosyluronic acid (uronic acid), made by extracting food-grade tissues from animal tissues (i.e., porcine intestine, bovine lung). [19], [20]. Has the highest negative charge density of any known biological macromolecule due to the numerous sulfate and carboxylic acid group [21]. It was hypothesized that since heparin has a particularly high negative charge that enables it to electrostatically interact with positively charged substances to produce nanoparticles [22], it might increase electrostatic repulsions between adjacent nanoparticles to reduce aggregation.

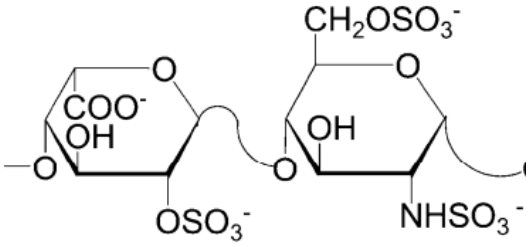

Figure 2. 4- Chemical structure of heparin [19].

2.1.5. RHODAMINE B

Rhodamine B isothiocyanate was purchased from Laborspirit (ref. 283924).

Rhodamine B isothiocyanate is an amphoteric dye, although because it contains a positive charge, it is usually categorized as a basic dye. It is a red dye of the xanthene family that is extremely water soluble [23]. Its chemical structure is shown in **Figure 2.5**. Rhodamine B, between several fluorescent dyes, is one of the most commonly utilized due to its simple conjugation reaction via isothiocyanate [24].

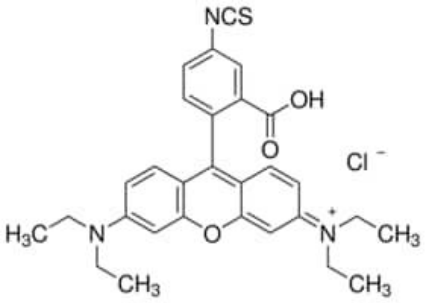

Figure 2. 5- Chemical structure of rhodamine B isothiocyanate [23].

2.2. METHODS

2.2.1. SYNTHESIS AND CHARACTERIZATION OF CALCIUM CARBONATE NANOTEMPLATES

$CaCO_3$ particles were produced using different processes that involved the coprecipitation of $CaCl_2$ and Na_2CO_3 aqueous solutions. Different salt concentrations and stirring times were applied while using these techniques (**Figure 2.6**). Additionally, rhodamine was encapsulated.

Scanning electron microscopy (SEM) was used to confirm the geometry of the nanoparticles and dynamic light scattering (DLS) allowed to measure the nanoparticle dimensions and aspect ratio. Fluorescence and confocal microscopy were used to show the fluorescent molecules immobilized in the interior (rhodamine is fluorescent in the far-red spectrum). The surface charge of $CaCO_3$ was assessed by zeta potential measurements.

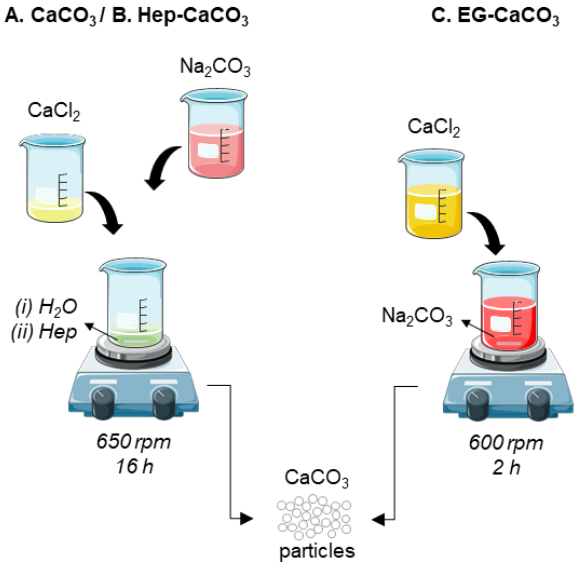

Figure 2. 6- Methods of preparation of $CaCO_3$ particles. In methods A and B, H_2O is used as solvent. H_2O or a solution of Hep are placed in the beaker where the coprecipitation is induced. $CaCl_2$ and Na_2CO_3 are added subsequently in this order. In method C, a mixture of 1:5 H_2O/EG is used as solvent. Na_2CO_3 is prepared first, onto which $CaCl_2$ is poured. $CaCO_3$ particles are obtained from all methods.

2.2.1.1. PURE $CACO_3$

To make pure $CaCO_3$, 5 M $CaCl_2$ and 1 M Na_2CO_3 solutions were first produced in distilled water. The reaction was then initiated by adding 650 µL $CaCl_2$ to 125 µL distilled water, followed by 2.5 mL Na_2CO_3. This mixture was regularly stirred at 650 rpm. 5 mL of distilled water was added after approximately 16 hours and stirring was stopped after 5 minutes.

2.2.1.2. HEP-$CaCO_3$

The above-described method was modified by replacing the 125 µL of distilled water by Hep solutions with concentrations ranging from 0.038 to 4.77 $mg \cdot mL^{-1}$. Hep-$CaCO_3$ loaded with Rho were produced by adding Rho to the Hep solution at a concentration of 100 $\mu g \cdot mL^{-1}$.

2.2.1.3. EG-$CaCO_3$

1 M Na_2CO_3 and 0.4 M $CaCl_2$ were first prepared in distilled water. For each solution, 1 mL was added to 10 mL of 1:5 H_2O:EG mixtures. Then, the mixture containing $CaCl_2$ was poured into the Na_2CO_3 mixture under agitation (600 rpm) and stopped after 30 s, 1 h, 1 h 30 min, 2 h, 3 h, 4 h and 24 h. EG-$CaCO_3$ was further loaded with Rho by adding 1 mL of 100 gmL^{-1} Rho to the Na_2CO_3 mixture.

2.2.2. MULTILAYER COATING OF THE NANOPARTICLES

The $CaCO_3$ nanoparticles were suspended successively in polyelectrolyte solutions – PLL and HA (2 mg/mL in 0.15 M NaCl) under mild agitation (250 rpm). After each deposition step, the nanoparticles were isolated from the solution by low-speed centrifugation (150 rcf, 3 min). The supernatant was removed with the aid of a micropipette and replaced by the next coating solution. The incubation with the polyelectrolytes was intercalated with NaCl for washing and removing loosely bonded polyelectrolytes. The procedure was repeated until 1, 2 and 3 bilayers were assembled. The coated nanoparticles were designated as "nanocapsules". The assembly of the coating was followed by measuring the zeta potential after each deposited layer, which showed a charge reversal corresponding to the sign of the last polyelectrolyte.

2.2.3. DRUG RELEASE

In vitro release profiles of Rho were examined at the same conditions of buffer, pH and temperature. After the EG-$CaCO_3$ synthesis, the NPs were stored in acidic PBS (6.3) and normal pH PBS (7.4). To produce this acidic PBS, the following reagents were added in the corresponding order and dissolved in 200mL of water gradually. First, we added 1.64g of NaCl and dissolved in 150mL of water. Then, we added 44.73mg of KCl, 60.76 mg of sodium phosphate dibasic (Na_2HPO_4) and in the last 188.61 mg of sodium phosphate monobasic (NaH_2). At the end, 50mL were added to make up the 200mL.

At 0h, 1h, 3h, 1 day, 3 days and 7 days, three 400µL aliquot were removed for quantification and dissolved in HCl. The fluorescence of the aliquots was measured to determine the remaining Rho. For this purpose, a fluorescence spectrometer was used to identify the maximum excitation/emission wavelengths at maximum peak. At all time-points, the leached mass of Rho was quantified, and the release profile compared to known drug release models: zero order (independent of the drug concentration), first order (directly proportional to the drug concentration), Higuchi (pure drug diffusion from a homogeneous matrix) and Korsmeyer-Peppas (dependent on diffusion and dynamic relaxation/swelling mechanisms), represented by Equations 1 to 4, respectively [25].

Zero-order release:

$$Q_t = Q_0 + K_0 t \qquad (1)$$

where Q_t is the cumulative amount of protein released at time t, Q_0 is the initial amount of protein and K_0 is the rate constant for the zero-order model.

First-order release:

$$\log(Q_t) = \log(Q_0) + \frac{Kt}{2.303} \qquad (2)$$

where Q_t is the cumulative amount of protein released at time t, Q_0 is the initial amount of protein and K is the rate constant for the first-order model.

Higuchi model release:

$$Q = K_H t^{1/2} \qquad (3)$$

where Q is the cumulative amount of protein released at time t and K_H is the rate constant for the Higuchi model.

Korsmeyer-Peppas model release:

$$M_t/M_\infty = Kt^n \qquad (4)$$

where M_t/M_∞ is the fraction of protein released at time t, K is the rate constant for the Korsmeyer model, and n is the exponent that characterizes the release mechanism.

Approximation of Rho release to these models is expected to reveal the phenomena governing the eventual coating defoliation or core dissolution.

2.2.4. *IN VITRO* CULTURE CELLS

Studies of cellular response were performed with the aim of evaluating the effect of the nanoparticles in two breast cancer cell lines: MDA-MB-231 and SK-BR-3 and a non-tumorigenic MCF10A breast epithelial cell line. These two cancer cell lines were selected due to their different aggressiveness: MDA-MB-231 have an aggressive phenotype, whereas SK-BR-3 are not aggressive. Cells were seeded on tissue culture polystyrene (15 000 cells/cm^2) and growth in Dulbecco's Modified Eagle Medium (DMEM) high glucose culture medium with 10% fetal bovine serum (FBS) and 1% antibiotics/antimycotics at 37°C and 5% CO_2. The medium was replaced every 2 or 3 days with fresh DMEM. When cell reach 80% of confluency, they were trypsinized (0.05% trypsin/0.53 mM EDTA (37 °C, 5% CO_2, 5 min) and cultured in contact with $CaCO_3$ nanoparticles (NPs suspension in culture media). Cells were seeded in 48 well plates (15000 cells·cm^2). After 24 h, approximately 4×10^8 uncoated or LbL-coated EG-$CaCO_3$ nanoparticles dispersed in 2.5 µL of PBS (pH 7.4) were added to each well containing 500 µL of medium, and incubated for 1, 2 and 3 days at 37 °C and 5% CO_2. All procedures from the synthesis of nanoparticles to their coating were performed in sterile conditions inside a laminar flow chamber and using filtered (cut off 0.22 µm) solutions.

2.2.5. METABOLIC ACTIVITY AND CELL VIABILITY

Metabolic activity and Live/Dead assays were performed after pre-determined culture periods (1, 2, and 3 days). To access cell metabolic activity, the AlamarBlue™ test- which contains the active agent resazurin - was performed by reading the fluorescence of this reagent in black 96-well plates (λ_{ex}=560 nm; λ_{em}=590 nm) using a microplate reader (Synergy HT, Bio-TEK, USA), after 4 h incubation. Three separate experiments were carried out, and each condition was assessed in triplicate. Statistical significance between groups was determined by one-way ANOVA and compared using the Shapiro-Wilks test (GraphPad Prism version 8.0.1, San Diego, CA). The levels of significance for statistical differences were set to $p<0.05$(*), $p<0.01$(**), and $p<0.001$(***).

Live/Dead assays showed the number of living and dead cells by staining with calcein AM (live, green) and propidium iodide (red, dead). Stained cells were observed by a confocal laser scanning microscope (CLSM, Zeiss AiryScan 2 model LSM 980, Germany).

2.2.6. $CaCO_3$ INTERNALIZATION WITH AND WITHOUT CD44 RECEPTOR BLOCKAGE

The internalization of uncoated and LbL-coated EG-$CaCO_3$ nanoparticles was evaluated 24 h after the nanoparticles were added to the culture. (CLSM, Zeiss AiryScan 2 model LSM 980, Germany). Because Rho fluoresces in the red spectrum, it was possible to see the nanoparticles and identify where they were located. To probe if the internalization is CD44-dependent, the CD44 receptors were blocked by CD44 blocking antibody (KM201, Abcam). Twenty-four hours after seeding (15000 cells·cm^{-2}) cell monolayers were incubated with 200 µL of complete DMEM supplemented with the CD44 blocking antibody (10 µg·mL^{-1}) at 37 °C in a 5% CO_2 atmosphere. After 30 min, the cells were washed with PBS and nanoparticles were added, as previously described. Because HA plays important roles in TME, we also assessed the effect of the nanoparticles on HA expression (staining with labelled lectin FITC-WGA, green) and visualized the particles embedment within pericellular HA (CLSM, Zeiss AiryScan 2 model LSM 980, Germany). To confirm the pericellular HA coating, MDA-MB-231 and SK-BR-3 cells were seeded on TCPS. After 48h, which corresponds to the time for analysis of WGA staining (after incubation with NPs), cells were fixed with 10% buffered formalin (1 h, 4 °C), and stained with biotinylated HA binding protein from bovine nasal cartilage (1 µg/mL, 1 h at room temperature, Millipore) followed by incubation with streptavidin-AlexaFluor® 488 conjugate (1 µg/mL, 10 min room temperature, Molecular Probes). Images were acquired using an Inverted confocal microscope (TCS SP8, Leica).

2.3. CHARACTERIZATION TECHNIQUES

Throughout this project, some characterization techniques were used. This section focuses on a brief description of these techniques.

2.3.1. DYNAMIC LASER SCATTERING (DLS)

DLS uses a laser on dissolved solutions to analyze the scattered light to reveal their size-(**Figure 2.7**) [26]. By the measurement of Brownian motion, DLS relates this with size distribution. To the movement of particles due to random impact with molecules of a liquid that encloses the particle we called Brownian motion. An important detail about Brownian motion is that large particles tend to move slowly while small particles move quickly [27]. Through the Stokes–Einstein equation, which relates the size of a particle and its speed, it is possible to calculate the size of a particle [28].

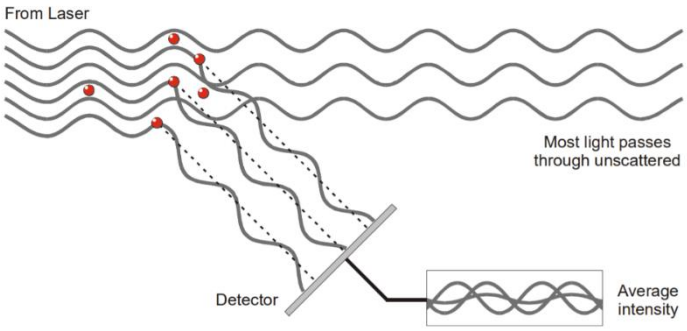

Figure 2. 7- Scheme of Dynamic Light Scattering [27].

2.3.2. SCANNING ELECTRON MICROSCOPE (SEM)

SEM is known for its large magnification reaching 300000x, where details and complexity that are invisible by light microscopy can be shown through this technique [29]. It depends on electron emission, produced by an electron gun [29], [30]. Then, the anode plate accelerates the electrons and magnetic lens focuses them. The scanning coils force the electron beam to rapidly scan over an area of the specimen. Finally, the sample can be viewed in Backscattered or secondary mode via a monitor [31]. SEM is an expensive technique, however it is useful because it provides a detailed grey-scale image of the sample analyzed for a wide range of materials.

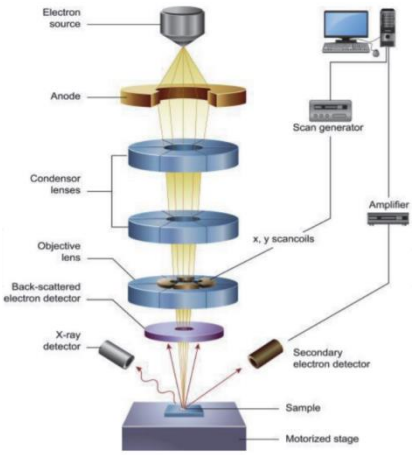

Figure 2. 8-Scheme of Scanning Electron Microscope [31].

2.3.3. FLUORESCENCE MICROSCOPY

In this technique, the sample intended to be examined is excited through a light with a specific wavelength, usually ultraviolet (UV) or blue. Through the barrier filter that absorbs the short wavelength light used for illumination and transmits the fluorescence, the sample is analyzed, seen as a glow through the black background. Due to the observation of fluorescence in a dark background, it can also be seen where the fluorescent components are [32], [33].

The main use is to treat samples with unique fluorescent reagents to examine them. These reagents can absorb light at a specific wavelength and emit light at different wavelengths, more towards the red spectrum area. For example, when the blue light is absorbed, green light will be emitted, green will be emitted yellow, yellow will be red and invisible UV will emit visible blue light [34].

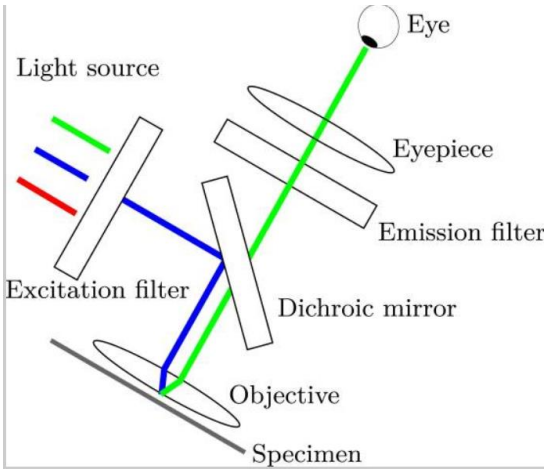

Figure 2. 9-Scheme of fluorescence microscope [34].

2.3.4. CONFOCAL MICROSCOPY

In confocal microscopy, a light source, often a laser, is reflected by a dichroic mirror or beam splitter and focused by an objective lens at the "Plane of Focus" level [35]. A confocal pinhole helps the microscope reject fluorescent light that is out of focus. The principle of this mechanism is that the image derives from a thin section and, when it scans various thin sections through the sample, it provides a very sharp three-dimensional image of the sample analyzed [36]. Due to its quick and inexpensive ability to acquire large tissue samples, confocal microscopy has enabled a significant advancement in biological imaging. This often includes fluorescence imaging, which is increasingly employed as a fundamental technique in biological research. Additionally, compared to pictures created by standard light microscopes, they can often have higher sensitivity, contrast, and resolution [35].

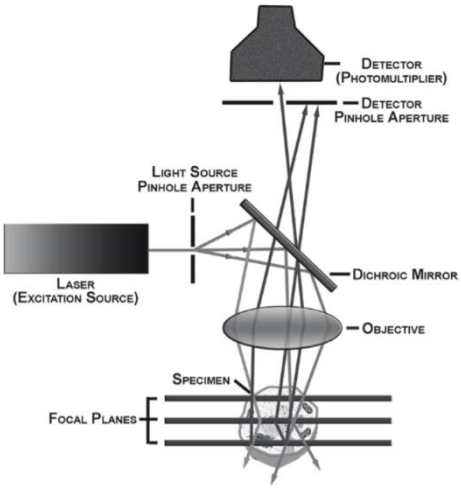

Figure 2. 10- Scheme of confocal microscopy [36].

2.3.5. ALAMAR BLUE ASSAYS

AlamarBlue is a fluorescent dye that contains an oxidation-reduction (REDOX) indicator that fluoresces and changes color in response to the chemical reduction of growth medium caused by cell growth (**Figure 2.11**). The alamarBlue test is developed to quantitatively evaluate the proliferation of diverse human and animal cell lines, bacteria and fungus- by colorimetric and/or fluorometric readings- and qualitative—a noticeable shift in color indicating the presence or absence of live cells [37], [38]. It is straightforward to execute since the indicator is water soluble, avoiding the washing/fixing and extraction procedures necessary in other frequently used cell proliferation assays [39]. Compared to standard cell viability/metabolic activity tests, the alamarBlue Assay has a number of benefits: due to its colorimetric and fluorescent properties, it provides a variety of detection techniques, being the most sensitive technique. Additionally, because there are fewer phases in the process, it can save time and it is simple to adapt [39].

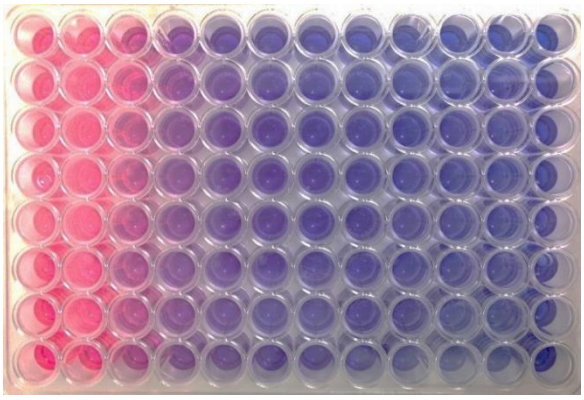

Figure 2. 11- Example of a plate from an AlamarBlue trial. Image from Oz Biosciences.

2.4. REFERENCES

[1] C. E. Schanté, G. Zuber, C. Herlin, and T. F. Vandamme, "Chemical modifications of hyaluronic acid for the synthesis of derivatives for a broad range of biomedical applications," *Carbohydr. Polym.*, vol. 85, no. 3, pp. 469–489, 2011.

[2] N. M. Salwowska, K. A. Bebenek, D. A. Żądło, and D. L. Wcisło-Dziadecka, "Physiochemical properties and application of hyaluronic acid: a systematic review," *J. Cosmet. Dermatol.*, vol. 15, no. 4, pp. 520–526, 2016.

[3] A. M. Vasi, M. I. Popa, M. Butnaru, G. Dodi, and L. Verestiuc, "Chemical functionalization of hyaluronic acid for drug delivery applications," *Mater. Sci. Eng. C*, vol. 38, no. 1, pp. 177–185, 2014.

[4] I. Caon *et al.*, "Revisiting the hallmarks of cancer: The role of hyaluronan," *Semin. Cancer Biol.*, vol. 62, no. July, pp. 9–19, 2020.

[5] E. Karousou *et al.*, "Roles and targeting of the HAS/hyaluronan/CD44 molecular system in cancer," *Matrix Biol.*, vol. 59, pp. 3–22, 2017.

[6] G. E. S. Chaudhry, A. Akim, M. N. Zafar, N. Safdar, Y. Y. Sung, and T. S. T. Muhammad, "Understanding hyaluronan receptor (CD44) interaction, HA-CD44 activated potential targets in cancer therapeutics," *Adv. Pharm. Bull.*, vol. 11, no. 3, pp. 426–438, 2021.

[7] I. S. Bayer, "Hyaluronic acid and controlled release: A review," *Molecules*, vol. 25, no. 11, 2020.

[8] H. Zhu, R. Liu, Y. Shang, and L. Sun, "Polylysine complexes and their biomedical applications," *Eng. Regen.*, vol. 4, no. 1, pp. 20–27, 2023.

[9] M. Zheng *et al.*, "Poly(α-L-lysine)-based nanomaterials for versatile biomedical applications: Current advances and perspectives," *Bioact. Mater.*, vol. 6, no. 7, pp. 1878–1909, 2021.

[10] I. C. Lee, Y. C. Wu, E. M. Cheng, and W. T. Yang, "Biomimetic niche for neural stem cell differentiation using poly-L-lysine/hyaluronic acid multilayer films," *J. Biomater. Appl.*, vol. 29, no. 10, pp. 1418–1427, 2015.

[11] M. S. Niepel, B. K. Ekambaram, C. E. H. Schmelzer, and T. Groth, "Polyelectrolyte

multilayers of poly (l-lysine) and hyaluronic acid on nanostructured surfaces affect stem cell response," *Nanoscale*, vol. 11, no. 6, pp. 2878–2891, 2019.

[12] V. Z. Prokopovic, A. S. Vikulina, D. Sustr, E. M. Shchukina, D. G. Shchukin, and D. V. Volodkin, "Binding Mechanism of the Model Charged Dye Carboxyfluorescein to Hyaluronan/Polylysine Multilayers," *ACS Appl. Mater. Interfaces*, vol. 9, no. 44, pp. 38908–38918, 2017.

[13] G. Amato *et al.*, "Hyaluronan/poly-l-lysine/berberine nanogels for impaired wound healing," *Pharmaceutics*, vol. 13, no. 1, pp. 1–11, 2021.

[14] H. Yue, Y. Zhao, X. Ma, and J. Gong, "Ethylene glycol: Properties, synthesis, and applications," *Chem. Soc. Rev.*, vol. 41, no. 11, pp. 4218–4244, 2012.

[15] R. K. Ibrahim, M. Hayyan, M. A. AlSaadi, S. Ibrahim, A. Hayyan, and M. A. Hashim, "Physical properties of ethylene glycol-based deep eutectic solvents," *J. Mol. Liq.*, vol. 276, pp. 794–800, 2019.

[16] B. V. Parakhonskiy, A. Haase, and R. Antolini, "Sub-micrometer vaterite containers: Synthesis, substance loading, and release," *Angew. Chemie - Int. Ed.*, vol. 51, no. 5, pp. 1195–1197, 2012.

[17] E. M. Flaten, M. Seiersten, and J. P. Andreassen, "Polymorphism and morphology of calcium carbonate precipitated in mixed solvents of ethylene glycol and water," *J. Cryst. Growth*, vol. 311, no. 13, pp. 3533–3538, 2009.

[18] D. B. Trushina, T. V. Bukreeva, M. V. Kovalchuk, and M. N. Antipina, "CaCO3 vaterite microparticles for biomedical and personal care applications," *Mater. Sci. Eng. C*, vol. 45, pp. 644–658, 2014.

[19] B. Casu, "Structure and Biological Activity of Heparin," *Adv. Carbohydr. Chem. Biochem.*, vol. 43, no. C, pp. 51–134, 1985.

[20] R. J. Linhardt, "2003 Claude S. Hudson award address in carbohydrate chemistry. Heparin: Structure and activity," *J. Med. Chem.*, vol. 46, no. 13, pp. 2551–2564, 2003.

[21] A. Onishi, K. St Ange, J. S. Dordick, and R. J. Linhardt, "Heparin and anticoagulation," *Front. Biosci. - Landmark*, vol. 21, no. 7, pp. 1372–1392, 2016.

[22] M. M. Kemp and R. J. Linhardt, "Heparin-based nanoparticles," vol. 1, pp. 77–87, 2010.

[23] A. El-Bindary, Z. Anwar, and T. El-Shafaie, "Effect of silicon dioxide nanoparticles on the assessment of quercetin flavonoid using Rhodamine B Isothiocyanate dye," *J. Mol. Liq.*, vol. 323, p. 114607, 2021.

[24] S. Hu *et al.*, "Tumor-specific fluorescence activation of rhodamine isothiocyanate derivatives," *J. Control. Release*, vol. 330, no. August 2020, pp. 842–850, 2021.

[25] R. R. Costa, C. A. Custódio, F. J. Arias, J. C. Rodríguez-Cabello, and J. F. Mano, "Nanostructured and thermoresponsive recombinant biopolymer-based microcapsules for the delivery of active molecules," *Nanomedicine Nanotechnology, Biol. Med.*, vol. 9, no. 7, pp. 895–902, 2013.

[26] S. Falke and C. Betzel, "Dynamic Light Scattering (DLS)," 2019, pp. 173–193.

[27] M. Instruments, *Zetasizer Nano User Manual MAN0485*. 2013.

[28] F. Babick, "Dynamic light scattering (DLS)," in *Characterization of Nanoparticles: Measurement Processes for Nanoparticles*, Elsevier, 2019, pp. 137–172.

[29] A. Mohammed and A. Abdullah, "SCANNING ELECTRON MICROSCOPY (SEM): A REVIEW," 2018.

[30] R. F. Egerton, *Physical Principles of Electron Microscopy*, vol. 56. New York: Springer, 2005.

[31] A. Salman Ali, "Application of Nanomaterials in Environmental Improvement," in *Nanotechnology and the Environment*, IntechOpen, 2020.

[32] Firas Mualla, Marc Aubreville, and Andreas Maier, *Microscopy*, Springer., vol. Chapter 5. Medical Imaging Systems: An Introductory Guide [Internet]., 2018.

[33] F. Rost, "Fluorescence microscopy, applications," in *Encyclopedia of Spectroscopy and Spectrometry*, Elsevier, 2016, pp. 627–631.

[34] "Principles and Application of Fluorescence Microscopy," 1998.

[35] P. J. Rigby and R. G. Goldie, "Confocal microscopy in biomedical research," *Croat. Med. J.*, vol. 40, no. 3, pp. 346–352, 1999.

[36] W. D. Swaim, "Overview of confocal microscopy.," *Methods Mol. Biol.*, vol. 588, pp. 187–201, 2010.

[37] S. N. Rampersad, "Multiple applications of alamar blue as an indicator of metabolic function and cellular health in cell viability bioassays," *Sensors (Switzerland)*, vol. 12, no. 9, pp. 12347–12360, 2012, doi: 10.3390/s120912347.

[38] R. D. Crackling, D. I. N. Iso, and G. Scuff, "Technical Datasheet Technical Datasheet," no. August, pp. 50–51, 2014.

[39] Invitrogen, "alamarBlue ® Assay," *US Pat. No 5501959*, no. 5, pp. 1–27, 2007.

CHAPTER 3.

LAYER-BY-LAYER COATED CALCIUM CARBONATE NANOPARTICLES FOR THE TARGETING OF BREAST CANCER CELLS[1]

[1] This chapter is based on the manuscript: Filipa R. Bastos, Diana Soares da Costa, Rui L. Reis, Natália M. Alves, Iva Pashkuleva, Rui R. Costa. *Layer-by-Layer Coated Calcium Carbonate Nanoparticles for the Specific Targeting of Breast Cancer Cells*. 2023. submitted to *Pharmaceutics*.

CHAPTER 3- LAYER-BY-LAYER COATED CALCIUM CARBONATE NANOPARTICLES FOR TARGETING BREAST CANCER CELLS

3.1. ABSTRACT

Breast cancer is resistant to conventional cancer treatments due to the specific tumor microenvironment, the associated acidic pH and overexpression of receptors enhancing cells tumorigenicity. In this work, we optimized the synthesis of acidic resorbable calcium carbonate ($CaCO_3$) nanoparticles and encapsulation of a low molecular weight model molecule (Rhodamine, Rho). The addition of ethylene glycol during the synthetic process resulted in formation of homogeneous $CaCO_3$ particles with average size of 564 nm. Their negative charge enabled the assembly of a layer-by-layer (LbL) coating with surface-exposed hyaluronic acid (HA), a known ligand of tumor-associated receptor CD44. The LbL coating controlled the release of the encapsulated drug: a two-fold decreased Rho release was observed when compared to uncoated nanoparticles. We further demonstrated the effect of the coated and uncoated nanoparticles on two breast cancer cell lines with different aggressiveness, namely SK-BR-3 and the more aggressive MDA-MB-231, and compared it with normal breast cell line MCF10A. The metabolic activity of the breast cancer cell lines was significantly decreased by $CaCO_3$ nanoparticles (coated and uncoated). Moreover, we found that the interactions between LbL-coated nanoparticles and cells depended on HA expression on the cell surface: more coated particles were observed on the surface of MDA-MB-231 cells which had the thickest HA coating. We concluded that $CaCO_3$ nanoparticles are potential candidates to carry low molecular weight chemotherapeutics and deliver them to aggressive breast cancer tumor sites with an HA-abundant pericellular matrix.

1.5. INTRODUCTION

Breast cancer is one of the most malignant diseases among women. In 2020, 11.7% of all diagnosed cancers were female breast cancer, making it the most prevalent cancer type in the world, followed by lung (11.4%) and colorectal cancers (10.0%) [1]. There are different subtypes of breast cancer that are categorized according to the expression of three typical hormone receptors: estrogen receptor (ER), progesterone receptor (PR), and human epidermal growth factor receptor-2 (HER2) [2]–[4]. Luminal A breast cancer is ER and PR positive; luminal B breast cancer is ER positive and depends on the HER2 status; and the triple-negative breast cancer (TNBC) is the most aggressive subtype, in which none of these typical receptors is expressed. Currently, several treatments are clinically used but they all have limitations: i) chemotherapy, which consists in the administration of anticancer drugs, fails when tumors

acquire drug resistance [5]; ii) radiotherapy uses radiation to kill tumorigenic cells but it is unselective and affects also healthy cells [6]; iii) hormone treatments targeting the typical breast cancer markers can be less effective than chemotherapy and is not applicable in the case of TNBC [7], [8].

The efficiency of the treatment can be improved if the therapy addresses the complexity of the tumor microenvironment (TME), especially in tumors that develop resistant and aggressive phenotypes. In breast cancer tumors, a high glycolytic cell metabolism results in the acidification of the TME to pH of 6.3-6.9 [9]–[11]. Calcium carbonate ($CaCO_3$) is an inorganic and biocompatible material that is stable at neutral pH but dissolves in acids [12]–[14]. $CaCO_3$ particles can be obtained by fast, effective and affordable methods that involve coprecipitation of calcium and carbonate ions in aqueous solution. Proteins and other molecules can be encapsulated in $CaCO_3$ particles with high efficiency by their simple addition to the reaction medium [15]–[17]. For example, doxorubicin, an anticancer drug, can be encapsulated in $CaCO_3$ particles and released in a pH responsive manner: it releases 20 times faster in acidic environments than at neutral pH [18]. Because the acidic pH in endolysosomes can also trigger the intracellular degradation of $CaCO_3$ [19], $CaCO_3$ particles are good candidates for cancer treatment.

$CaCO_3$ particles are negatively charged and thus, can be used as templates for electrostatic-driven layer-by-layer (LbL) deposition – an alternating adsorption of oppositely charged building blocks onto a substrate [20]–[22]. The LbL method discards the need of chemical modification and use of aggressive solvents. It can be applied to coat substrates with any geometry under mild conditions (temperature, pressure and pH), therefore allowing the use of sensitive, bioactive blocks that can enhance the efficiency of the targeted drug delivery to eukaryotic cells and bacteria [23], [24].

In this work, we optimized the synthesis of $CaCO_3$ nanoparticles and their modification by LbL coating. To this end, we chose polyanionic hyaluronic acid (HA) as a bioactive building block for the coatings. HA is a natural ligand of CD44 receptor that is overexpressed in different cancers, including breast cancer. CD44 and HA interact via the basic arginines Arg41 and Arg78 of the receptor and the carboxyl groups of HA [25]. Accumulation of HA in TME and overexpression of CD44 by cancer cells is associated with high invasiveness, stemness, and metastatic potential [26]–[28]. Previous studies with LbL films containing HA have demonstrated the utility of these constructs in understanding and manipulating the interactions between HA and CD44 [29], [30]. Herein, we investigated the potential of pH-sensitive $CaCO_3$ nanoparticles LbL-coated with HA to target breast cancer cells with different metastatic potential, and the dependence of the efficiency on the expression of CD44.

3.1. MATERIALS AND METHODS

1.5.1. MATERIALS

Calcium chloride anhydrous ($CaCl_2$), heparin sodium salt from porcine intestinal mucosa (Hep, grade I-A, ≥180 USP units/mg), sodium chloride (NaCl), poly-L-lysine hydrobromide (PLL, molecular weight 15–30 kDa, determined by viscosity), rhodamine B isothiocyanate (Rho), antibiotic antimycotic solution (100×, stabilized with 10000 units penicillin and 10 mg streptomycin), phosphate buffered saline (PBS, in tablets), potassium chloride (KCl), sodium phosphate dibasic (Na_2HPO_4), sodium phosphate monobasic (NaH_2PO_4), Dulbecco's Modified Eagle Medium (DMEM) high glucose with 4500 mg·L^{-1} glucose, L-glutamine, and sodium bicarbonate, without sodium pyruvate were purchased from Sigma-Aldrich. Sodium carbonate anhydrous (Na_2CO_3, calcein AM, and trypsin/EDTA (0.05% trypsin/0.53 mM EDTA) were purchased from VWR. Sodium hyaluronate (21–40 kDa) was purchased from Lifecore biomedical. Ethylene glycol (>99.5%, for analysis) was purchased from Carlo Erba. Fetal bovine serum (FBS, qualified, one-shot format), propidium iodide, and wheat germ agglutinin (WGA) labeled with fluorescein isothiocyanate (FITC) were purchased from Alfagene. Deep Blue Cell Viability™ kit was purchased from Lusopalex. Anti-CD44 antibodies KM201 were obtained from Abcam.

1.5.2. SYNTHESIS OF CALCIUM CARBONATE PARTICLES

$CaCO_3$ particles were synthesized by $CaCl_2$ and Na_2CO_3 coprecipitation at different conditions. 5 M $CaCl_2$ and 1 M Na_2CO_3 solutions were prepared in distilled water. Aliquot of 650 µL of $CaCl_2$ solution was diluted with 125 µL of distilled water, followed by addition of 2.5 mL Na_2CO_3 solution and stirring at 650 rpm for 16 h. Then we added 5 mL of distilled water and stopped the agitation after 5 min. For the preparation of heparin-doped $CaCO_3$ (*i.e.,* Hep-$CaCO_3$), the method was adapted from Ueno *et al.* [31]. Briefly, the above described method was modified by replacing the 125 µL of distilled water by Hep solutions with concentrations ranging from 0.038 to 4.77 mg·mL^{-1} (**Appendix I**). Hep-$CaCO_3$ loaded with Rho were produced by adding Rho to the Hep solution at a concentration of 100 µg·mL^{-1}. The method to prepare $CaCO_3$ in ethylene glycol (*i.e.,* EG-$CaCO_3$) was adapted from Parakhonskiy *et al.* [32]. 1 M Na_2CO_3 and 0.4 M $CaCl_2$ were first prepared in distilled water. For each solution, 1 mL was added to 10 mL of 1:5 H_2O:EG mixtures. Then, the mixture containing $CaCl_2$ was poured into the Na_2CO_3 mixture under agitation (600 rpm) and stopped after 30 s, 1 h, 1 h 30 min, 2 h, 3 h, 4 h and 24 h (**Appendix II**). EG-$CaCO_3$ were also loaded with Rho by adding 1 mL of 100 µg·mL^{-1} Rho to the solution of Na_2CO_3.

1.5.3. DIMENSIONS AND MORPHOLOGY OF CALCIUM CARBONATE PARTICLES

The diameters of $CaCO_3$, Hep-$CaCO_3$, and EG-$CaCO_3$ particles were determined in wet state by dynamic light scattering (DLS, Malvern Nano-ZS equipment with a He–Ne laser at an angle of 173°) using aliquots with 1 mL loaded in polystyrene disposable cuvettes. The polydispersity index (PDI), the size distribution and z-average were determined by fitting the correlation function with the cumulant method (Zetasizer Nano v7.10 software). The presented data are average values from 35 measurements. Dry $CaCO_3$ particles were observed by a scanning electron microscope (SEM, JEOL-JSM-6010LV, Japan). After preparation, the particles were centrifuged for 3 min at 1500 rpm and washed in ultrapure water. A 100 µL drop of each $CaCO_3$ formulation was dispensed on glass, placed on SEM holder, and left drying for 24 h at 37 °C. The particles were then sputtered with gold and placed in the SEM sample chamber.

1.5.4. LAYER-BY-LAYER COATING OF CALCIUM CARBONATE NANOPARTICLES

EG-$CaCO_3$ nanoparticles were washed with 0.15 M NaCl and suspended alternately in 2 $mg \cdot mL^{-1}$ solutions of PLL and HA prepared in 0.15 M NaCl under mild agitation (250 rpm) for 10 min. Each deposition step was intercalated with a washing step in 0.15 M NaCl, and for each deposition/washing step the nanoparticles were retrieved from suspension by low-speed centrifugation (1500 rpm, 3 min). The supernatant was removed with the aid of a micropipette and replaced by the next coating/washing solution. The procedure was repeated until 3 PLL/HA bilayers were assembled. The deposition of each polyion was followed by measuring the zeta (ζ)-potential of the nanoparticles using folded capillary cuvettes and the Nano-ZS equipment (Malvern, UK).

1.5.5. *IN VITRO* RELEASE OF RHODAMINE

The *in vitro* release of Rho from nanoparticles (uncoated and coated with one PLL/HA bilayer) was followed at 37 °C in PBS solution with pH 6.3 (140 mM NaCl, 3 mM KCl, 2 mM Na_2HPO_4, 8 mM NaH_2PO_4). The nanoparticles were suspended in 12 mL of PBS and aliquots of 400 µL were taken at pre-determined time-points: 0 h, 1 h, 3 h, 1 day, 3 days, and 7 days. The $CaCO_3$ in the aliquots was dissolved with 3 mL of 1 M HCl to release the remaining (*i.e.*, not released) Rho. The fluorescence was measured in a fluorescence spectrophotometer (JASCO model FP-8500, Japan) using an excitation wavelength of 564 nm (determined from the maximum absorbance peak of a 50 $\mu g \cdot mL^{-1}$ Rho solution (**Appendix III**)) and emission interval between 575 nm and 650 nm. The intensity of the emitted fluorescence was read

at 585 nm and compared to a calibration curve of known Rho concentrations (**Appendix IV**). The cumulative release was represented as a percentage of the total encapsulated mass of Rho, measured at 0 h. The release profile was fitted to several known models: zero-order, first-order, Higuchi, and Korsmeyer-Peppas models to determine the mass transport mechanism involved in Rho release.

1.5.6. *IN VITRO* CELL CULTURE

MDA-MB-231 and SK-BR-3 epithelial breast cancer cell lines and a non-tumorigenic MCF10A breast epithelial cell line were obtained from the American Type Culture Collection (ATCC). For expansion, cells were routinely cultured on 75 cm^2 tissue culture polystyrene flasks with high glucose DMEM supplemented with 10% FBS and 1% antibiotics/antimycotics in an incubator at 37 °C and a humidified air atmosphere with 5% CO_2. The medium was replaced every 2 or 3 days with fresh DMEM. When cells reached 80% of confluence, they were detached with 0.05% trypsin/0.53 mM EDTA (37 °C, 5% CO_2, 5 min). The trypsin was inactivated by adding complete medium, and the cells were centrifuged at 300*g* for 5 min. Cells were resuspended in DMEM for a new expansion or transferred to well plates for incubation experiments with $CaCO_3$ nanoparticles. In the latter case, cells were first seeded in 48 well plates (15000 cells·cm^{-2}). After 24 h, approximately 4×10^8 uncoated or LbL-coated EG-$CaCO_3$ nanoparticles dispersed in 2.5 µL of PBS (pH 7.4) were added to each well containing 500 µL of medium, and incubated for 1, 2 and 3 days at 37 °C and 5% CO_2. All procedures from the synthesis of nanoparticles to their coating were performed in sterile conditions inside a laminar flow chamber and using filtered (cut off 0.22 µm) solutions.

1.5.7. METABOLIC ACTIVITY AND CELL VIABILITY

Metabolic activity and Live/Dead assays were performed after pre-determined culture periods (1, 2, and 3 days). Metabolic activity was assessed by the AlamarBlue™ test – which contains the active agent resazurin – following the supplier's instructions. Resazurin is reduced to the highly fluorescent resofurin in living cells. After 4 h incubation, the fluorescence was measured in black 96-well plates (λ_{ex}=560 nm; λ_{em}=590 nm) using a microplate reader (Synergy HT, Bio-TEK, USA). Three independent experiments were performed and each condition was measured in triplicate. Statistical significance between groups was determined by one-way ANOVA and compared using the Shapiro-Wilks test (GraphPad Prism version 8.0.1, San Diego, CA). The levels of significance for statistical differences were set to $p<0.05$(*), $p<0.01$(**), and $p<0.001$(***).

Live/Dead assays were performed by staining living and dead cells with calcein AM (green) and propidium iodide (red), respectively. Stained cells were observed by a confocal laser scanning microscope (CLSM, Zeiss AiryScan 2 model LSM 980, Germany).

1.5.8. $CaCO_3$ INTERNALIZATION WITH AND WITHOUT CD44 RECEPTOR BLOCKAGE

The internalization of uncoated and LbL-coated EG-$CaCO_3$ nanoparticles was assessed 24 h after the addition of the nanoparticles to the culture (CLSM, Zeiss AiryScan 2 model LSM 980, Germany). Rho is fluorescent in the red spectrum and allowed visualization of the nanoparticles and determination of their localization. To probe if the internalization is CD44-dependent, the CD44 receptors were blocked by CD44 blocking antibody (KM201, Abcam). Twenty-four hours after seeding (15000 cells·cm^{-2}) cell monolayers were incubated with 200 µL of complete DMEM supplemented with the CD44 blocking antibody (10 µg·mL^{-1}) at 37 °C in a 5% CO_2 atmosphere. After 30 min, the cells were washed with PBS and nanoparticles were added, as previously described. Because HA plays important roles in TME, we also assessed the effect of the nanoparticles on HA expression (staining with labelled lectin FITC-WGA, green) and visualized the particles embedment within pericellular HA (CLSM, Zeiss AiryScan 2 model LSM 980, Germany). To confirm the pericellular HA coating, MDA-MB-231 and SK-BR-3 cells were seeded on TCPS. After 48h, which corresponds to the time for analysis of WGA staining (after incubation with NPs), cells were fixed with 10% buffered formalin (1 h, 4 °C), and stained with biotinylated HA binding protein from bovine nasal cartilage (1 µg/mL, 1 h at room temperature, Millipore) followed by incubation with streptavidin-AlexaFluor® 488 conjugate (1 µg/mL, 10 min room temperature, Molecular Probes). Images were acquired using an Inverted confocal microscope (TCS SP8, Leica).

1.6. RESULTS AND DISCUSSION

1.6.1. SYNTHESIS AND CHARACTERIZATION OF CALCIUM CARBONATE NANOPARTICLES

The properties of $CaCO_3$ obtained by coprecipitation depend on the reaction conditions. Particles with different dimensions, shapes and crystallinity can be obtained from subtle changes in the time and velocity of agitation, Ca^{2+}/CO_3^{2-} ratios, and the addition of doping agents, among others [33]. When using a simple coprecipitation of $CaCl_2$ and Na_2CO_3 in water (*i.e.,* without any additives), $CaCO_3$ particles with diameters between 2–10 µm are obtained [34]–[36]. Recent studies suggest that $CaCO_3$ precipitation is

slower when Ca^{2+} is in excess compared to CO_3^{2-} [37], which may result in formation of smaller particles. We used a Ca^{2+}:CO_3^{2-} ratio of 5:1 and SEM showed formation of $CaCO_3$ crystals with different dimensions, most of them around 700 nm (**Figure 3.1A1**). However, in aqueous media these particles had diameter of around 3.6 µm, which demonstrates a tendency to aggregate (**Figure 3.1A2**).

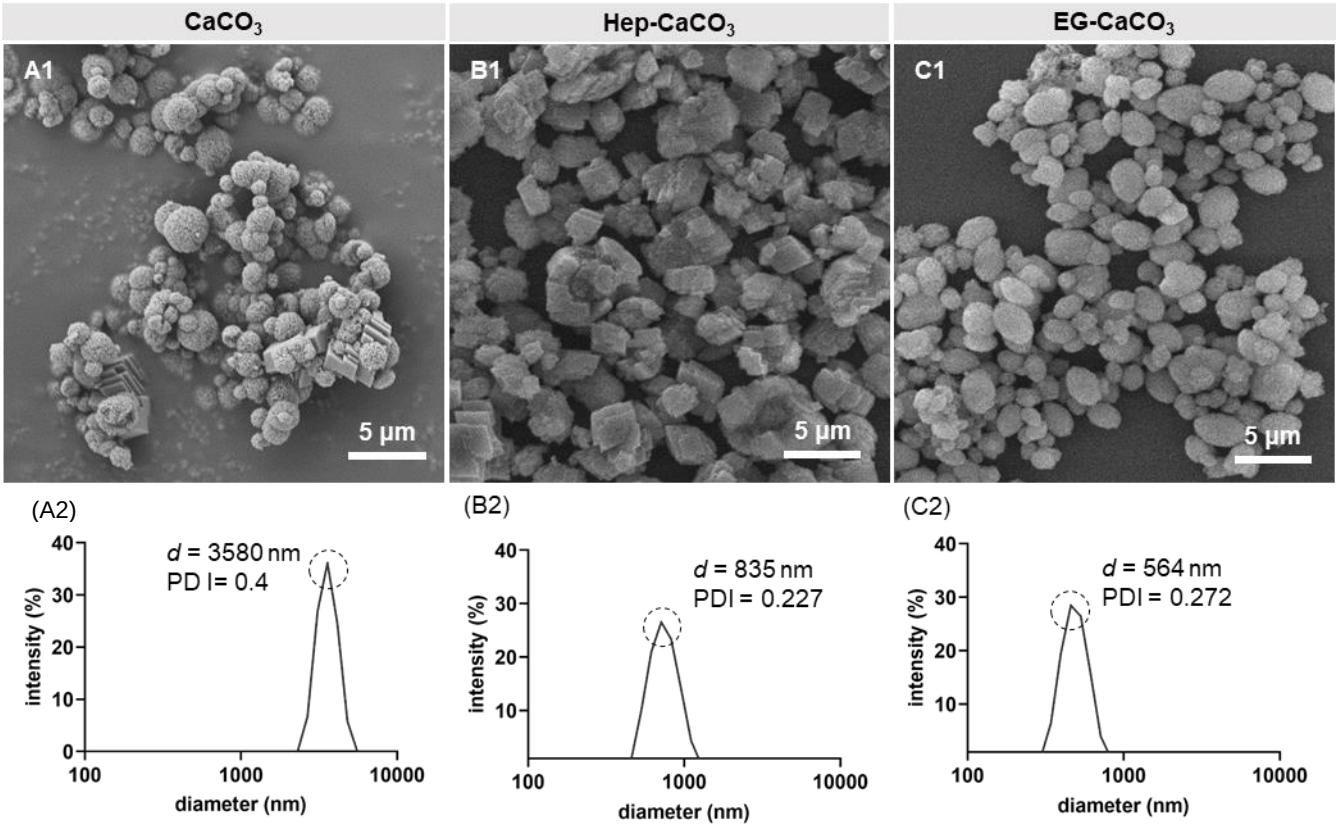

Figure 3. 1- SEM micrographs (A1, B1, C1) and representative size distribution of $CaCO_3$, Hep-$CaCO_3$ and EG-$CaCO_3$ determined by DLS (A2, B2, C2). The values shown in the DLS graphs correspond to the diameter (d) and PDI of the distribution peak.

To avoid aggregation, we added a charged polymer to the reaction to induce electrostatic repulsion between the particles. We chose Hep because it is the natural polyelectrolyte with highest negative charge and already used in clinics [38], [39]. First, we determined the influence of Hep on the size of the particles within a wide range of concentrations (**Appendix I**). As expected, the increasing quantities of Hep led to a systematic decrease of the particles diameter (from 2.7 µm for 0.038 mg·mL^{-1} Hep to 835 nm for 4.77 mg·mL^{-1} Hep) and PDI, which showed avoided aggregation (**Figures 3.1B1, 3.1B2**). Most of the obtained nanoparticles were rhombohedral. This shape is typically found in calcite particles, one of the most stable $CaCO_3$ polymorphs [40], demonstrating that Hep has a stabilizing structural effect.

We also tested EG as an additive because previous studies have shown that EG can slow down the reaction and crystal growth [32]. To optimize the reaction time, we monitored the particles size during 24 h (**Appendix II**). Within 2 h, we obtained monodisperse particles with a diameter around 564 nm and an ellipsoid shape (**Figures 3.1C1, 3.1C2**), *i.e.*, EG-$CaCO_3$ nanoparticles were smaller than $CaCO_3$ and Hep-$CaCO_3$ particles.

Particles with a diameter below 1 µm (submicron scale) can be internalized by breast cancer cells [41]. The capacity of Hep-$CaCO_3$ and EG-$CaCO_3$ particles to carry low molecular weight therapeutics was investigated by encapsulating the model fluorophore Rho (≈500 Da) during the coprecipitation. The amount of the encapsulated Rho in each $CaCO_3$ system was quantified by dissolving the particles in 1 M HCl: we obtained 50.4 µg of Rho per mole of $CaCO_3$ in Hep-$CaCO_3$ and 130.5 µg per mole of $CaCO_3$ in EG-$CaCO_3$, *i.e.*, the amount of Rho was 3-fold higher in EG-$CaCO_3$ particles. The effect of Rho on the size of Hep-$CaCO_3$ and EG-$CaCO_3$ was also assessed and the DLS analysis showed a significant increase of Hep-$CaCO_3$ diameter (**Figure 3.2A,** only 36% of the Rho-loaded particles were in the submicron scale), while the size of EG-$CaCO_3$ was not altered significantly (**Figure 3.2B,** 100% all particles had a diameter below 1 µm). We therefore selected EG-$CaCO_3$ nanoparticles for the following experiments.

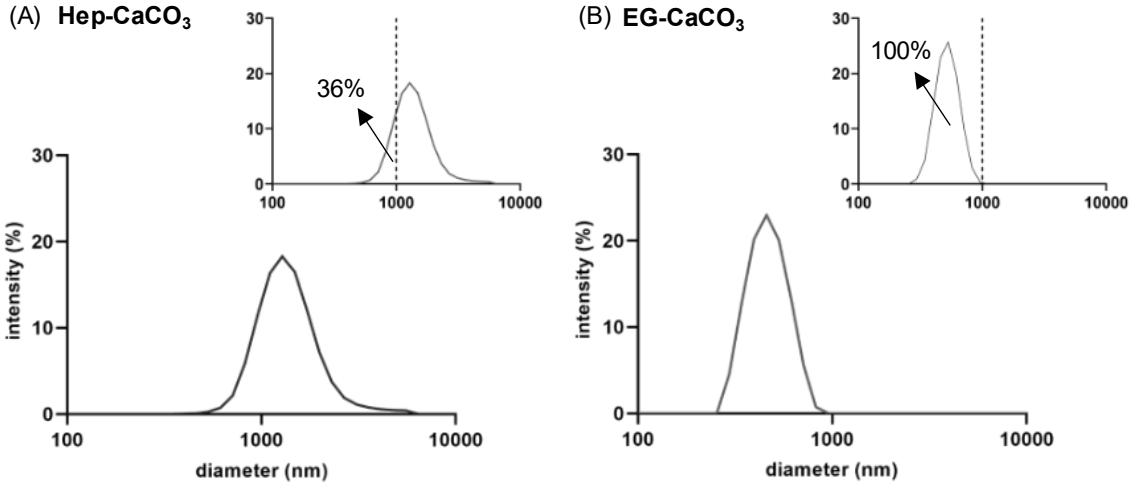

Figure 3. 2- Size distribution of (A) Hep-$CaCO_3$ and (B) EG-$CaCO_3$ loaded with Rho. The main graphs show one representative distribution graph. The insets show the average distribution calculated from 35 measurements.

1.6.2. LAYER-BY-LAYER COATING AND RHODAMINE RELEASE

We used Rho-loaded EG-$CaCO_3$ nanoparticles (ζ-potential about -6 mV) as templates to assemble a LbL coating that endows CD44 targeting and control the release rate. Up to three bilayers of PLL and HA were assembled (**Figure 3.3A**). The polyanionic HA was the bioactive building block in this composition, whereas the polycationic PLL was employed as polycation that allowed electrostatic stabilization of the LbL build-up. The deposition of PLL and HA was confirmed by variation of the particles charge. Our results agree with previous data showing partial compensation of PLL charge by HA (ζ-potential increase upon PLL deposition but does not become positive) and involvement not only of electrostatic interactions but also of other supramolecular interactions (*e.g.*, hydrogen bonds) in the assembly of this polyelectrolyte pair [42].

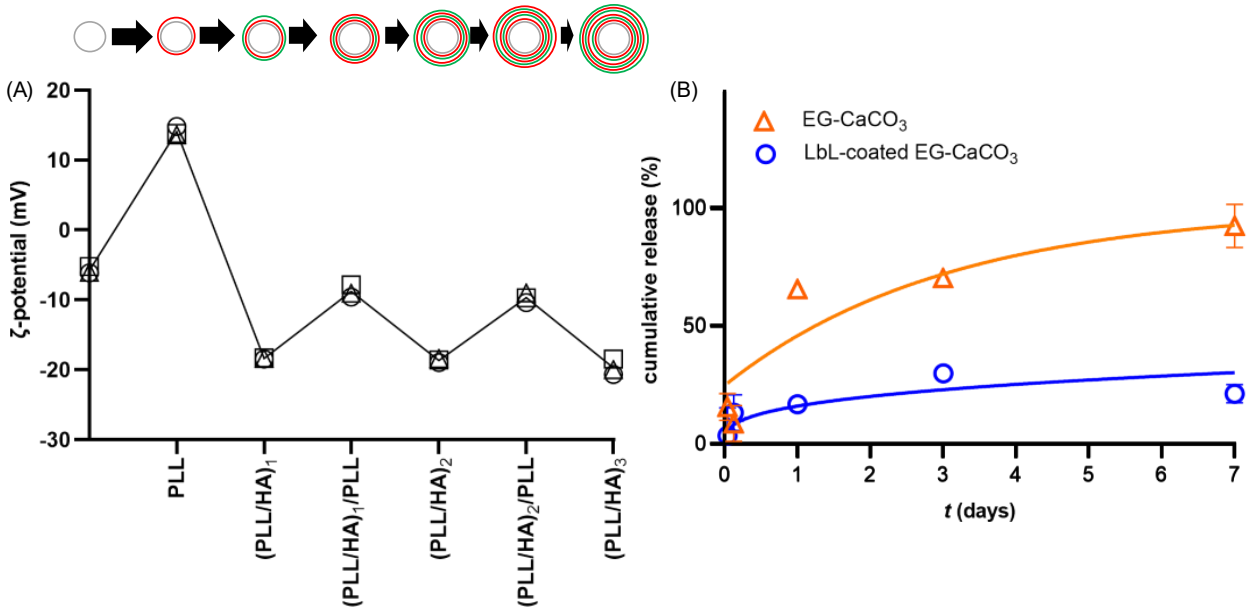

Figure 3. 3- A) Zeta-potential of the surface of Rho-loaded EG-$CaCO_3$ nanoparticles. The cartoons represent nanoparticles coated with incremental numbers of layers. Three individual measurements are represented per layer. The line is a visual guide for the variation of the average zeta-potential values. (B) Cumulative release of Rho from uncoated (Δ, orange) and LbL-coated EG-$CaCO_3$ (□, blue) nanoparticles at pH 6.3 for 7 days. The curves are fittings to first-order (uncoated) and Korsmeyer-Peppas (coated) release models. Data are means ± one standard deviation. Some error bars are too small to be seen.

The release of Rho from uncoated and LbL-coated nanoparticles was studied in an aqueous environment that mimics the acidic pH of the TME (pH=6.3). We used nanoparticles coated with only one PLL/HA bilayer because of the long LbL deposition times. By choosing a low number of layers, the coating time is shortened and a premature release due to long processing times is reduced. The data showed that uncoated EG-$CaCO_3$ released 65% of Rho within 1 day, while only 17% of Rho was released from the

LbL-coated nanoparticles for the same period (**Figure 3.3B**). Within 3 days, these values increased to 70% and 30%, respectively, and did not change substantially until 7 days. Such a substantial difference (more than 2-fold) confirms that one PLL/HA bilayer was sufficient to slow the release. It is likely that the coating worked not only as a physical barrier between the nanoparticle and the medium but also as a buffer protecting the nanoparticle against dissolution. Of note, the release at neutral pH (pH=7.4) was significantly lower than at acidic conditions: only 10% of Rho were released from the coated nanoparticles after 3 days, evidencing the expected pH response from $CaCO_3$ systems (**Appendix V**).

To better understand the Rho release, the data were fitted to different drug release models (**Appendix VI**). Data for uncoated EG-$CaCO_3$ fitted well to a first-order model of release, *i.e.*, Rho release decreased with time and was only dependent on the concentration of Rho within the nanoparticle. This is the expected behavior from water-soluble drugs released from inert porous matrices. For the LbL-coated nanoparticles, we found a better approximation to a Korsmeyer-Peppas model, which describes the release from dynamic polymeric matrices such as hydrogels. This model confirms the role of LbL in controlling the release of encapsulated molecules and agrees, with the data obtained for other LbL-coated $CaCO_3$ particles [43].

1.6.3. INTERACTION OF EG-$CaCO_3$ NANOPARTICLES WITH BREAST CANCER CELLS

The biological impact of uncoated and LbL-coated EG-$CaCO_3$ nanoparticles was investigated on epithelial breast cancer cells with different expression of CD44. MDA-MB-231 cells are aggressive and invasive phenotype that overexpress CD44, while SK-BR-3 cells have a basal expression of this receptor and are considered non-invasive [44]–[47]. MCF10A cells are used as a model for normal human mammary epithelial cells and have a low CD44 expression mainly detected in the cytoplasm [48]. We assessed the cytotoxicity of EG-$CaCO_3$ with and without LbL coating and found no cytotoxic effect for the tested cell lines (**Figure 3.4, Appendix VII**).

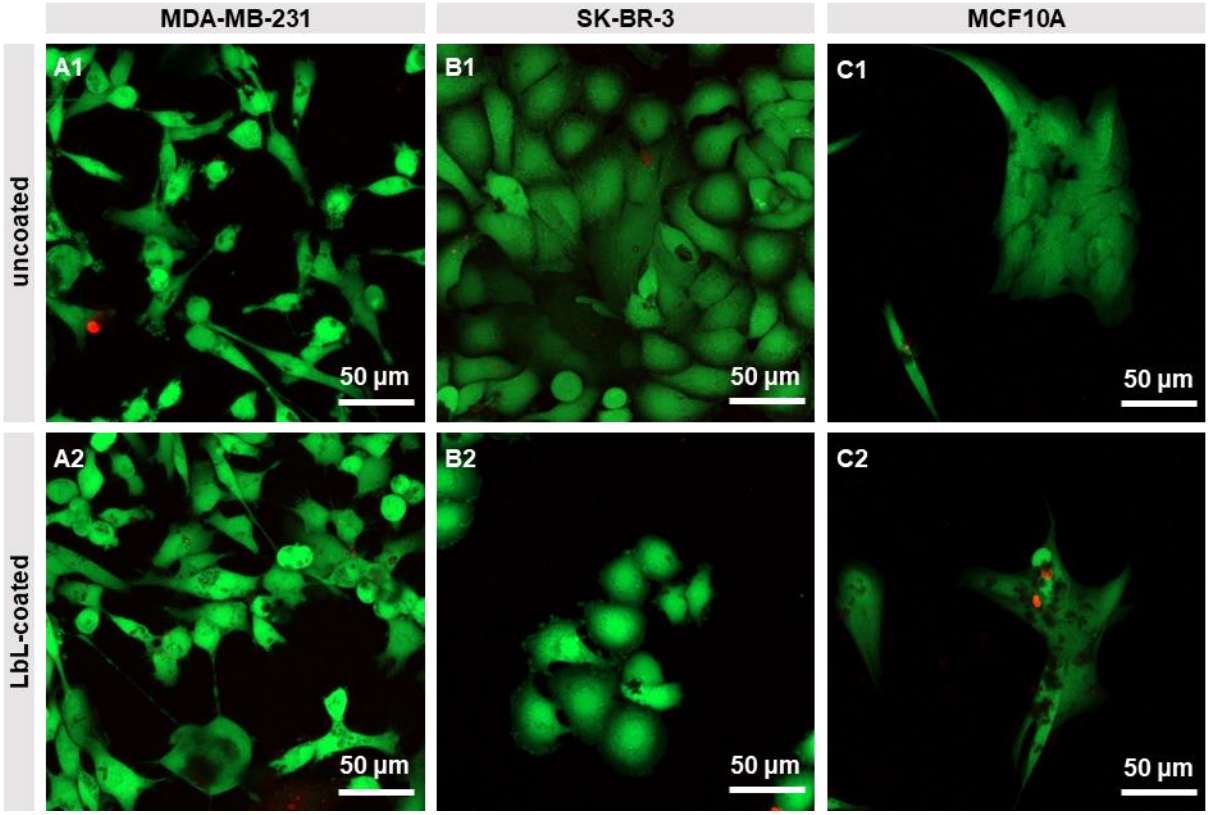

Figure 3. 4- Live/Dead assay of (A) MDA-MB-231, (B) SK-BR-3, and (C) MCF10A cell lines incubated with uncoated and LbL-coated EG-$CaCO_3$ nanoparticles for 3 days (green: live; red: dead). The small red dots correspond to the nanoparticles loaded with Rho.

Despite the cells being alive, their metabolism was affected by the nanoparticles (**Figure 3.5**). The metabolic activity of MDA-MB-231 and SK-BR-3 cells significantly decreased with culture time when compared to the control. After 2 days of incubation with the uncoated EG-$CaCO_3$ nanoparticles the metabolic activity of MDA-MB-231 (70.4%) and SK-BR-3 cells (81.2%) decreased whereas MCF10A cells (88.7%) were not affected significantly. At day 3, the decrease in the metabolic activity of MDA-MB-231 and SK-BR-3 cells decreased further (64.4% and 73.4%, respectively), showing that these nanoparticles affect both phenotypes. The LbL coating vanished partially this effect at short culture time (1 day). At longer culture times (2 and 3 days), we observed a decrease of the metabolic activity for the breast cancer cell lines, but not for the normal cell line, MCF10A, *i.e.*, the effect was similar to the uncoated particles. This delay in the response can be due to different interactions between cells and the coated nanoparticles that triggers different internalization mechanisms when compared with uncoated particles and/or different rate of the particles dissolution in the lysosome as shown by the Rho release data.

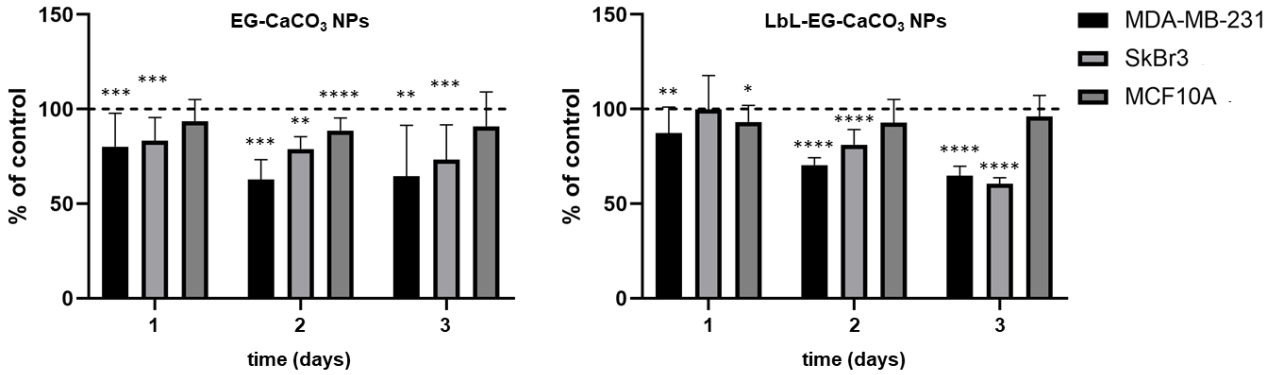

*Figure 3. 5- Effect of uncoated and LbL-coated EG-$CaCO_3$ nanoparticles (NPs) on metabolic activity of MDA-MB-231, SK-BR-3 and MCF10A cell lines after 1, 2 and 3 days of incubation. Data are presented as a percentage of control (i.e., cells cultured without nanoparticles, dashed line corresponds to the control). Statistical differences are represented between each sample and its control for the different days with n=3. Significant differences are indicated (*p<0.05; **p<0.01; ***p<0.001).*

To analyze the nanoparticles' distribution in the pericellular space and in the cells' cytoplasm we observed the cultures by CLSM. After 1 day, uncoated EG-$CaCO_3$ were found mainly around the cells with very few internalized (**Appendix VIII**). At days 2 and 3, internalization was observed for all studied cell types (**Figure 3.6**), regardless of the CD44 expression level. The results for the LbL-coated EG-$CaCO_3$ nanoparticles were different - most of the particles remained attached to MDA-MB-231 and SK-BR-3 cancer cells, even after 3 days, with only few being internalized. Because we did not observe differences between MDA-MB-231 and SK-BR-3 cells (different expression of CD44), we hypothesized that the endogenous HA creates a protective pericellular coat that engages the expressed CD44 and retains the coated nanoparticles [49]. Lectin binding experiments showed higher HA deposition in the pericellular matrix of MDA-MB-231 than of SK-BR-3 cells and mainly intracellular HA in the case of MCF10A cells (**Appendix IX**). Indeed, we observed more nanoparticles around MDA-MB-231 than around SK-BR-3 cells, which agrees with the ticker HA coat around MDA-MB-231 when compared to SK-BR-3 (**Appendix X**) [47].

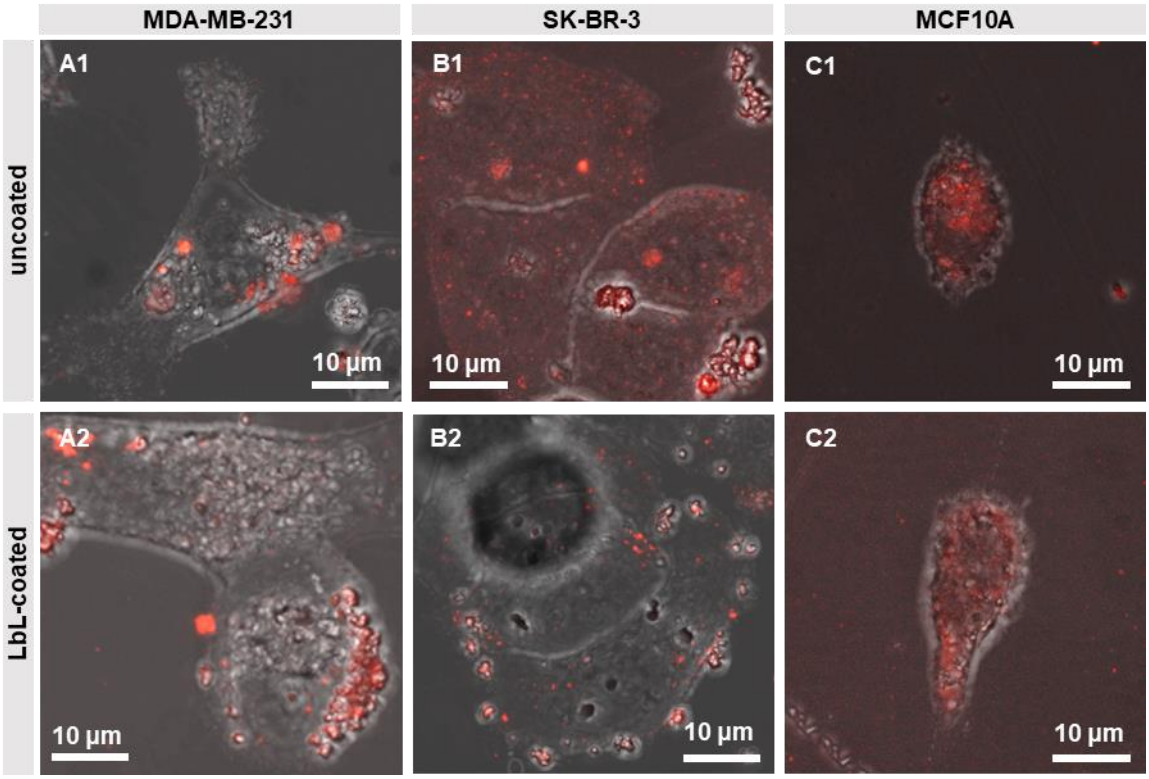

Figure 3. 6- Distribution of uncoated and LbL-coated EG-$CaCO_3$ nanoparticles after 3 days of incubation with (A) MDA-MB-231, (B) SK-BR-3, and (C) MCF10A cell lines (red: Rho).

To understand if CD44 was involved in the internationalization of the nanoparticles, we blocked this receptor before incubation of the cells with the nanoparticles. Upon CD44 blocking, we observed enhanced internalization of uncoated and coated nanoparticles by all studied cell types after 24 h (**Figure 3.7**). Interestingly, this enhanced internalization was concomitant with different distribution of the non-internalized coated nanoparticles in the pericellular space of cancer cells - they were organized in discrete clusters (**Figure 3.7A2-ii**, **3.7B2-ii**) but not homogeneously distributed as observed in cells without CD44 blocking (**Figure 3.7A4-ii**, **3.7B4-ii**). This difference was very pronounced for MDA-MB-231 cells. On one hand, CD44 blocking can affect the HA turnover and compromise the HA coat around the cells. On the other hand, we have recently demonstrated that the receptor for hyaluronan mediated motility (RHAMM) can compensate the blocked CD44 and make cells more sensitive to exogenous supplemented HA [46]. These results show that although CD44 receptors are not directly involved in the internalization of the nanoparticles, their presence is important because of their interactions with endogenous HA.

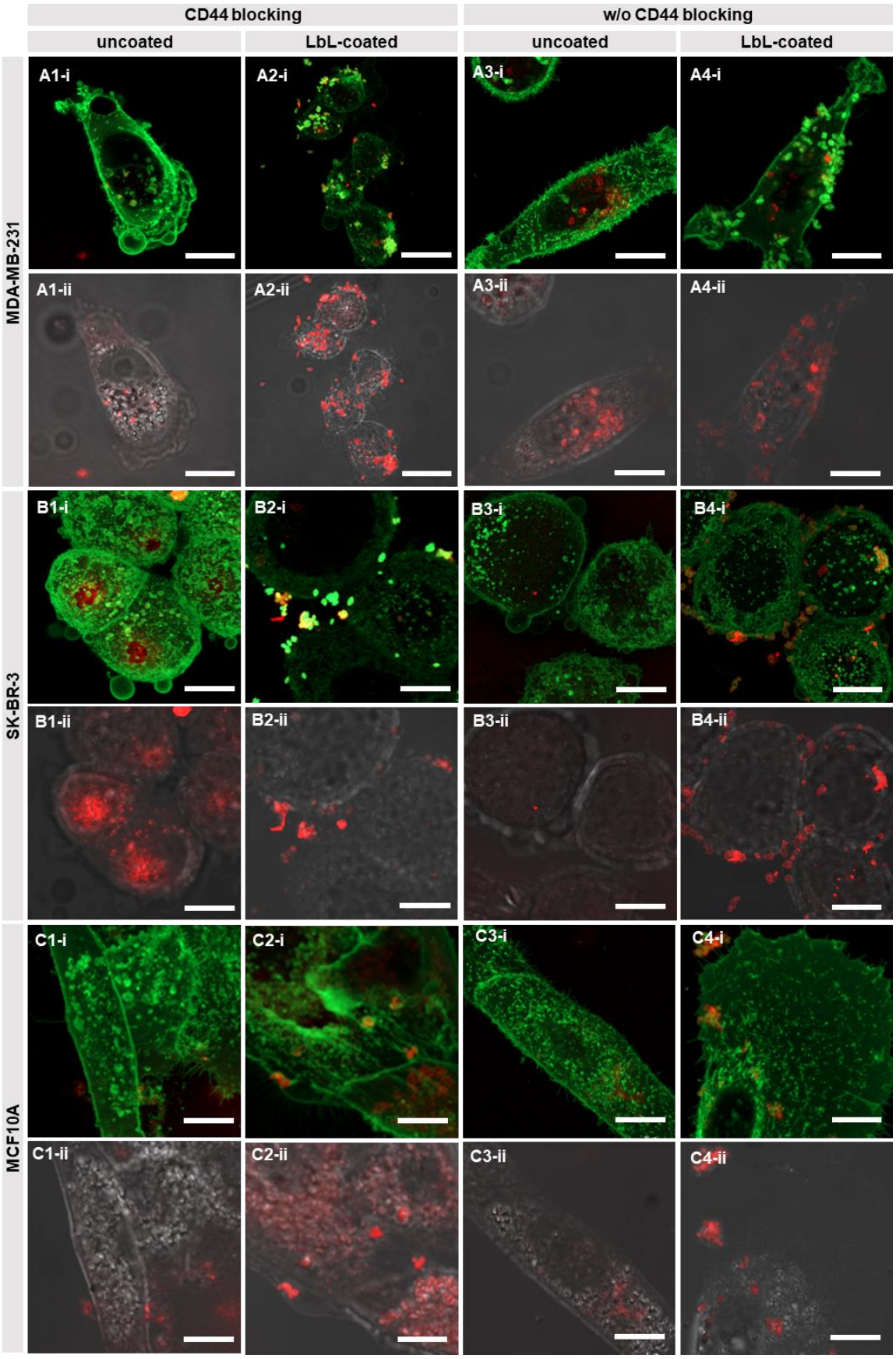

Figure 3. 7- Distribution of uncoated and LbL-coated EG-$CaCO_3$ nanoparticles after 24 h of incubation with (A) MDA-MB-231, (B) SK-BR-3, and (C) MCF10A cell lines with and without CD44 blocking (red: Rho, green: cell membrane glycoproteins). Scale bars: 10 µm.

1.7. CONCLUSIONS

In this work we demonstrated that $CaCO_3$ are promising platform for the treatment of breast cancer because of their pH responsiveness and negative charge that allows LbL deposition. The LbL coating controls the rate of $CaCO_3$ resorption at acidic pH and thus, the release of the encapsulated agent but also discriminates the nanoparticles interactions with cancer cells and non-tumorigenic cells: LbL coating favors pericellular immobilization of nanoparticles over their internalization by cells with HA-rich matrix typical for cancer cells.

While we did not contemplate the use of therapeutic drugs, they can be loaded on demand during $CaCO_3$ coprecipitation, converting the nanoparticles into drug delivery systems. We envisage that the enhanced release observed in acidic conditions and pericellular immobilization can be combined to target specific surface receptors overexpressed in tumors and minimize unspecific delivery to healthy cells. Moreover, we suggest that future studies should focus on understanding the role of different HA receptors such as RHAMM in nanoparticles accumulation in the ECM.

1.8. ACKNOWLEDGMENTS

This research was funded by the Portuguese Fundação para a Ciência e Tecnologia (FCT, project number PTDC/CTM-REF/0022/2020) and the European program FEDER/FEEI. RRC and DSC acknowledge FCT for support through grants CEECIND/02842/2017 and SFRH/BPD/85790/2012.

1.9. REFERENCES

[1] H. Sung *et al.*, "Global Cancer Statistics 2020: GLOBOCAN Estimates of Incidence and Mortality Worldwide for 36 Cancers in 185 Countries," *CA. Cancer J. Clin.*, vol. 71, no. 3, pp. 209–249, 2021.

[2] S. Loibl, P. Poortmans, M. Morrow, C. Denkert, and G. Curigliano, "Breast cancer," *The Lancet*, vol. 397, no. 10286. Elsevier B.V., pp. 1750–1769, 2021.

[3] R. Erber and A. Hartmann, "Histology of Luminal Breast Cancer," *Breast Care*, vol. 15, no. 4. S. Karger AG, pp. 327–336, 2020.

[4] L. Yin, J. J. Duan, X. W. Bian, and S. C. Yu, "Triple-negative breast cancer molecular subtyping and treatment progress," *Breast Cancer Res.*, vol. 22, no. 1, pp. 1–13, 2020, doi:

10.1186/s13058-020-01296-5.

[5] H. E. Lee *et al.*, "An increase in cancer stem cell population after primary systemic therapy is a poor prognostic factor in breast cancer," *Br. J. Cancer*, vol. 104, no. 11, pp. 1730–1738, 2011.

[6] P. A. Williams, S. Cao, D. Yang, and R. L. Jennelle, "Patient-reported outcomes of the relative severity of side effects from cancer radiotherapy," *Support. Care Cancer*, vol. 28, no. 1, pp. 309–316, 2020.

[7] Y. Xie *et al.*, "Chemotherapy Shows a Better Efficacy Than Endocrine Therapy in Metastatic Breast Cancer Patients with a Heterogeneous Estrogen Receptor Expression Assessed by 18F-FES PET," *Cancers (Basel).*, vol. 14, no. 14, 2022, doi: 10.3390/cancers14143531.

[8] Q. Liu *et al.*, "Comparison of endocrine therapy and chemotherapy as different systemic treatment modes for metastatic luminal HER2-negative breast cancer patients —A retrospective study," *Front. Oncol.*, vol. 12, no. July, pp. 1–16, 2022, doi: 10.3389/fonc.2022.873570.

[9] Y. Zhang *et al.*, "High-resolution label-free 3D mapping of extracellular pH of single living cells," *Nat. Commun.*, vol. 10, no. 1, pp. 1–9, 2019, doi: 10.1038/s41467-019-13535-1.

[10] P. Swietach, R. D. Vaughan-Jones, A. L. Harris, and A. Hulikova, "The chemistry, physiology and pathology of pH in cancer," *Philos. Trans. R. Soc. B Biol. Sci.*, vol. 369, no. 1638, 2014, doi: 10.1098/rstb.2013.0099.

[11] M. Chen *et al.*, "Extracellular pH is a biomarker enabling detection of breast cancer and liver cancer using CEST MRI," *Oncotarget*, vol. 8, no. 28, pp. 45759–45767, 2017, doi: 10.18632/oncotarget.17404.

[12] C. Xu *et al.*, "Biodegradable Nanoparticles of Polyacrylic Acid–Stabilized Amorphous CaCO3 for Tunable pH-Responsive Drug Delivery and Enhanced Tumor Inhibition," *Adv. Funct. Mater.*, vol. 29, no. 24, 2019, doi: 10.1002/adfm.201808146.

[13] D. B. Trushina, T. N. Borodina, S. Belyakov, and M. N. Antipina, "Calcium carbonate vaterite particles for drug delivery: Advances and challenges," *Mater. Today Adv.*, vol. 14, no. 2022, p. 100214, 2022, doi: 10.1016/j.mtadv.2022.100214.

[14] Z. Dong *et al.*, "CaCO3 nanoparticles as an ultra-sensitive tumor-pH-responsive nanoplatform

enabling real-time drug release monitoring and cancer combination therapy," *Biomaterials*, vol. 110, pp. 60–70, 2016, doi: 10.1016/j.biomaterials.2016.09.025.

[15] V. L. Kudryavtseva, L. Zhao, S. I. Tverdokhlebov, and G. B. Sukhorukov, "Fabrication of PLA/CaCO3 hybrid micro-particles as carriers for water-soluble bioactive molecules," *Colloids Surfaces B Biointerfaces*, vol. 157, pp. 481–489, 2017, doi: 10.1016/j.colsurfb.2017.06.011.

[16] J. J. Richardson *et al.*, "Versatile Loading of Diverse Cargo into Functional Polymer Capsules," *Adv. Sci.*, vol. 2, no. 1–2, pp. 6–11, 2015, doi: 10.1002/advs.201400007.

[17] A. I. Petrov, D. V. Volodkin, and G. B. Sukhorukov, "Protein-calcium carbonate coprecipitation: A tool for protein encapsulation," *Biotechnol. Prog.*, vol. 21, no. 3, pp. 918–925, 2005, doi: 10.1021/bp0495825.

[18] S. A. Kamba, M. Ismail, S. H. Hussein-Al-Ali, T. A. T. Ibrahim, and Z. A. B. Zakaria, "In vitro delivery and controlled release of doxorubicin for targeting osteosarcoma bone cancer," *Molecules*, vol. 18, no. 9, pp. 10580–10598, 2013, doi: 10.3390/molecules180910580.

[19] C. Wang *et al.*, "Lipase-Triggered Water-Responsive 'Pandora's Box' for Cancer Therapy: Toward Induced Neighboring Effect and Enhanced Drug Penetration," *Adv. Mater.*, vol. 30, no. 14, pp. 1–10, 2018, doi: 10.1002/adma.201706407.

[20] C. Monge, J. Almodóvar, T. Boudou, and C. Picart, "Spatio-temporal control of LbL films for biomedical applications: From 2D to 3D," *Adv. Healthc. Mater.*, vol. 4, no. 6, pp. 811–830, 2015, doi: 10.1002/adhm.201400715.

[21] D. Alkekhia, P. T. Hammond, and A. Shukla, "Layer-by-Layer Biomaterials for Drug Delivery," *Annu. Rev. Biomed. Eng.*, vol. 22, pp. 1–24, 2020, doi: 10.1146/annurev-bioeng-060418-052350.

[22] R. R. Costa and J. F. Mano, "Polyelectrolyte multilayered assemblies in biomedical technologies," *Chem. Soc. Rev.*, vol. 43, no. 10, pp. 3453–3479, 2014, doi: 10.1039/c3cs60393h.

[23] C. Tan *et al.*, "Advanced CaCO3-derived delivery systems for bioactive compounds," *Adv. Colloid Interface Sci.*, vol. 309, no. September, p. 102791, 2022, doi: 10.1016/j.cis.2022.102791.

[24] F. Ali Said, N. Bousserrhine, V. Alphonse, L. Michely, and S. Belbekhouche, "Antibiotic loading and development of antibacterial capsules by using porous CaCO3 microparticles as starting material," *Int. J. Pharm.*, vol. 579, no. February, p. 119175, 2020, doi: 10.1016/j.ijpharm.2020.119175.

[25] M. Lintuluoto, Y. Horioka, S. Hongo, J. M. Lintuluoto, and Y. Fukunishi, "Molecular Dynamics Simulation Study on Allosteric Regulation of CD44-Hyaluronan Binding as a Force Sensing Mechanism," *ACS Omega*, vol. 6, no. 12, pp. 8045–8055, 2021, doi: 10.1021/acsomega.0c05502.

[26] K. Wu *et al.*, "CD44 correlates with clinicopathological characteristics and is upregulated by EGFR in breast cancer," *Int. J. Oncol.*, vol. 49, no. 4, pp. 1343–1350, 2016, doi: 10.3892/ijo.2016.3639.

[27] A. M. Carvalho, R. Teixeira, R. Novoa-Carballal, R. A. Pires, R. L. Reis, and I. Pashkuleva, "Redox-Responsive Micellar Nanoparticles from Glycosaminoglycans for CD44 Targeted Drug Delivery," *Biomacromolecules*, vol. 19, no. 7, pp. 2991–2999, 2018, doi: 10.1021/acs.biomac.8b00561.

[28] R. Thapa and G. D. Wilson, "The Importance of CD44 as a Stem Cell Biomarker and Therapeutic Target in Cancer," *Stem Cells International*, vol. 2016. Hindawi Limited, 2016.

[29] S. Amorim, I. Pashkuleva, C. A. Reis, R. L. Reis, and R. A. Pires, "Tunable layer-by-layer films containing hyaluronic acid and their interactions with CD44," *J. Mater. Chem. B*, vol. 8, no. 17, pp. 3880–3885, 2020, doi: 10.1039/d0tb00407c.

[30] V. Domínguez-Arca *et al.*, "Liposomes embedded in layer by layer constructs as simplistic extracellular vesicles transfer model," *Mater. Sci. Eng. C*, vol. 121, no. September 2020, p. 111813, 2021, doi: 10.1016/j.msec.2020.111813.

[31] Y. Ueno, H. Futagawa, Y. Takagi, A. Ueno, and Y. Mizushima, "Drug-incorporating calcium carbonate nanoparticles for a new delivery system," *J. Control. Release*, vol. 103, no. 1, pp. 93–98, 2005.

[32] B. Parakhonskiy *et al.*, "The influence of the size and aspect ratio of anisotropic, porous CaCO3 particles on their uptake by cells," *J. Nanobiotechnology*, vol. 13, no. 1, 2015.

[33] Y. Q. Niu *et al.*, "Calcium carbonate: controlled synthesis, surface functionalization, and nanostructured materials," *Chem. Soc. Rev.*, vol. 51, no. 18, pp. 7883–7943, 2022, doi: 10.1039/d1cs00519g.

[34] G. Yan *et al.*, "Stable and Biocompatible Cellulose-Based CaCO3 Microspheres for Tunable pH-Responsive Drug Delivery," *ACS Sustain. Chem. Eng.*, vol. 7, no. 24, pp. 19824–19831, 2019, doi: 10.1021/acssuschemeng.9b05144.

[35] D. V. Volodkin, A. I. Petrov, M. Prevot, and G. B. Sukhorukov, "Matrix Polyelectrolyte Microcapsules: New System for Macromolecule Encapsulation," *Langmuir*, vol. 20, no. 8, pp. 3398–3406, 2004, doi: 10.1021/la036177z.

[36] L. M. I. Schijven, V. Saggiomo, A. H. Velders, J. H. Bitter, and C. V. Nikiforidis, "On the influence of protein aggregate sizes for the formation of solid and hollow protein microparticles," *J. Colloid Interface Sci.*, vol. 631, pp. 181–190, 2023, doi: 10.1016/j.jcis.2022.11.007.

[37] S. Y. M. H. Seepma *et al.*, "Controlling CaCO3Particle Size with {Ca2+}:{CO32-} Ratios in Aqueous Environments," *Cryst. Growth Des.*, vol. 21, no. 3, pp. 1576–1590, 2021, doi: 10.1021/acs.cgd.0c01403.

[38] I. Capila and R. J. Linhardt, "Heparin - Protein Interactions," *Angew. Chem.* Int, vol. 41, no. 3, pp. 390–412, 2002, doi: 10.1002/1521-3773(20020201)41:3<390::aid-anie390>3.0.co;2-b.

[39] R. J. Weiss, J. D. Esko, and Y. Tor, "Targeting heparin and heparan sulfate protein interactions," *Org. Biomol. Chem.*, vol. 15, no. 27, pp. 5656–5668, 2017, doi: 10.1039/c7ob01058c.

[40] R. A. Boulos, F. Zhang, E. S. Tjandra, A. D. Martin, D. Spagnoli, and C. L. Raston, "Spinning up the polymorphs of calcium carbonate," *Sci. Rep.*, vol. 4, pp. 1–6, 2014, doi: 10.1038/srep03616.

[41] P. Foroozandeh and A. A. Aziz, "Insight into Cellular Uptake and Intracellular Trafficking of Nanoparticles," *Nanoscale Res. Lett.*, vol. 13, 2018, doi: 10.1186/s11671-018-2728-6.

[42] R. Teixeira, R. L. Reis, and I. Pashkuleva, "Influence of the sulfation degree of glycosaminoglycans on their multilayer assembly with poly-l-lysine," *Colloids Surfaces B Biointerfaces*, vol. 145, pp. 567–575, 2016, doi: 10.1016/j.colsurfb.2016.05.069.

[43] R. R. Costa, C. A. Custódio, F. J. Arias, J. C. Rodríguez-Cabello, and J. F. Mano, "Nanostructured and thermoresponsive recombinant biopolymer-based microcapsules for the delivery of active molecules," *Nanomedicine Nanotechnology, Biol. Med.*, vol. 9, no. 7, pp. 895–902, 2013, doi: 10.1016/j.nano.2013.01.013.

[44] C. Sheridan *et al.*, "CD44+/CD24-Breast cancer cells exhibit enhanced invase properties: An early step necessary for metastasis," *Breast Cancer Res.*, vol. 8, no. 5, pp. 1–13, 2006, doi: 10.1186/bcr1610.

[45] N. Sun, H. N. Xu, Q. Luo, and L. Z. Li, "Potential indexing of the invasiveness of breast cancer cells by mitochondrial redox ratios," *Adv. Exp. Med. Biol.*, vol. 923, pp. 121–127, 2016, doi: 10.1007/978-3-319-38810-6_16.

[46] A. M. Carvalho, D. Soares da Costa, R. L. Reis, and I. Pashkuleva, "RHAMM expression tunes the response of breast cancer cell lines to hyaluronan," *Acta Biomater.*, vol. 146, pp. 187–196, 2022, doi: 10.1016/j.actbio.2022.05.013.

[47] A. M. Carvalho, D. Soares da Costa, R. L. Reis, and I. Pashkuleva, "Influence of Hyaluronan Density on the Behavior of Breast Cancer Cells with Different CD44 Expression," *Adv. Healthc. Mater.*, vol. 11, no. 4, pp. 1–9, 2022, doi: 10.1002/adhm.202101309.

[48] J. Puleo and K. Polyak, "The MCF10 model of breast tumor progression," *Cancer Res.*, vol. 81, no. 16, pp. 4183–4185, 2021, doi: 10.1158/0008-5472.CAN-21-1939.

[49] E. A. Turley, D. K. Wood, and J. B. McCarthy, "Carcinoma Cell Hyaluronan as a 'Portable' Cancerized Pro- Metastatic Microenvironment," Cancer Res., vol. 76, no. 9, pp. 2507–2512, 2016, doi: 10.1158/0008-5472.CAN-15-3114.

Chapter 4.
General Conclusions

4.1. CONCLUSIONS AND FUTURE WORK

In this thesis, different procedures for $CaCO_3$ particle generation were employed and evaluated for as new localized breast cancer therapy systems. Since particles obtained by conventional precipitation procedures have a tendency to aggregate and are often too large to explore targeting and cell internalization (*i.e.*, in the order of few micrometers), the addition of Hep and EG helped mitigating the aggregation of the nanoparticles. Herein, more profound studies were conducted with EG-$CaCO_3$ nanoparticles since they demonstrated higher encapsulation efficiency than Hep-$CaCO_3$ nanoparticles and the dimensions of the systems was preserved in the submicrometric scale after loading with Rho. Crucial for this work was the demonstration that EG-$CaCO_3$ nanoparticles are suitable templates for depositing PLL and the CD44 targeting HA using the LbL technique. This technique was a convenient method for generating nanoparticle coatings thanks to the electrostatic attraction – and to some extent, hydrogen bonding – between the used polyelectrolytes and endow targeting ability.

The pH responsiveness of $CaCO_3$ was confirmed: release of the encapsulated Rho was faster in acidic medium, useful to control the release of drugs in the acidic TME. Moreover, the LbL coating helped in slowing down the release, which opens the possibility of tuning the release further in the future. Finally, it was shown that cancer cells with different metastatic potential were inhibited by the presence of EG-$CaCO_3$. Thanks to the surface-exposed HA, the nanoparticles interacted with the CD44 of the cells' ECM and accumulated in the pericellular region. On the other hand, blocking the CD44 receptors allowed the nanoparticles to enter the cells, leading to the conclusion that internalization is CD44-independent. These achievements are a good indicator of the feasibility of this project. Furthermore, since this work also demonstrates that healthy cells are largely unaffected by LbL-coated $CaCO_3$ nanoparticles, the potential therapeutic benefits for localized cancer treatments is evidenced.

This project opens the possibility to future work with chemotherapeutic substances already used in clinics and using more complex *in vitro* cancer models. One such possibility is the encapsulation of doxorubicin, a well-known cancer drug. The effect of this drug not only in 2D systems but also 3D cellular arrangements, *i.e.*, spheroids, is expected to further validate the use of these inorganic systems and the TME targeting properties of the LbL coating. Finally, observing that coated nanoparticles are immobilized in the pericellular space enables the local delivery of drugs to the TME, but raises the question about the mechanism of internalization. Other less studied receptors, such as RHAMM, may mediate internalization and should be investigated in greater detail so that nanoparticle systems can be modified to not only the ECM but also the intracellular environment.

CHAPTER 5.
APPENDIX

APPENDIX I

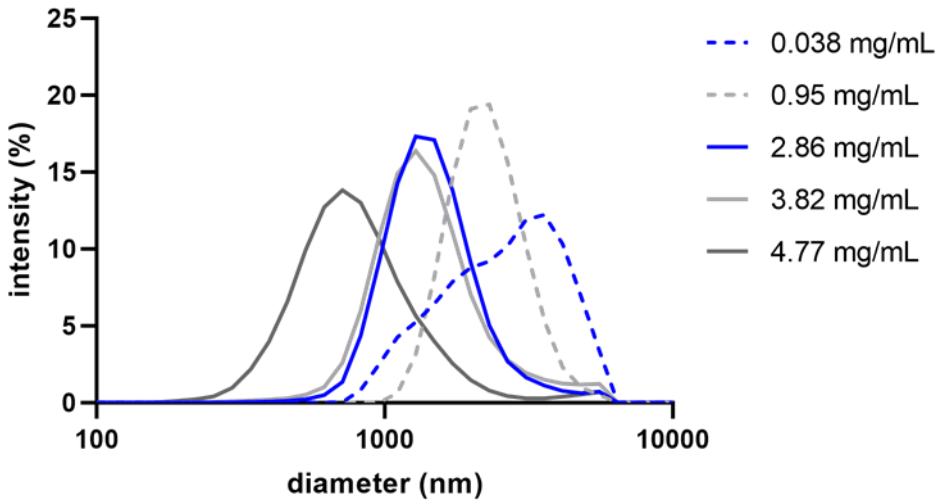

Figure S1. Size distribution of Hep-$CaCO_3$ with different concentrations of Hep. Results are the average of 35 independent measurements.

Table S1. Diameters and PDI of Hep-$CaCO_3$obtained with different concentrations of Hep. Results are the average of 35 independent measurements.

Hep concentration (mg/ml)	***PDI***	***diameter (nm)***
0.038 mg/mL	0.40 ± 0.337	2771 ± 1064
0.95 mg/mL	0.35 ± 0.309	2329 ± 477
2.86 mg/mL	0.18 ± 0.098	1539 ± 276
3.82 mg/mL	0.19 ± 0.121	1514 ± 382
4.77 mg/mL	0.23 ± 0.178	835 ± 196

APPENDIX II

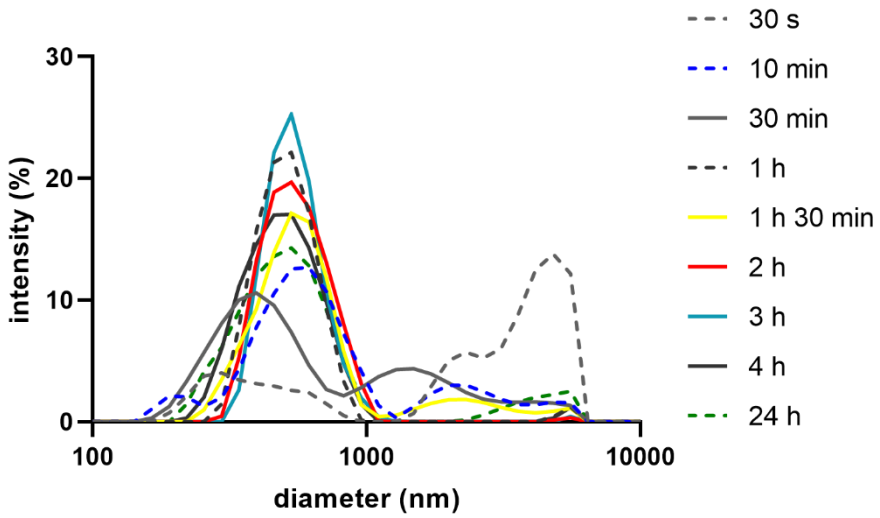

Figure S2. Size distributions of EG-$CaCO_3$ with different stirring times. Each curve represents the average of 5 independent measurements.

Table S2. Diameters and PDI of EG-$CaCO_3$ obtained with different stirring times of EG-$CaCO_3$. Results are the average of 5 independent measurements.

time	***PDI***	***diameter (nm)***
30 s	0.64 ± 0.314	3976 ± 968
10 min	0.45 ± 0.243	904 ± 745
30 min	0.34 ± 0.081	830 ± 555
1 h	0.20 ± 0.148	517 ± 74
1 h 30 min	0.23 ± 0.168	905 ± 766
2 h	0.27 ± 0.201	564 ± 108
3 h	0.28 ± 0.174	554 ± 87
4 h	0.25 ± 0.137	506 ± 129
24 h	0.37 ± 0.105	491 ± 145

APPENDIX III

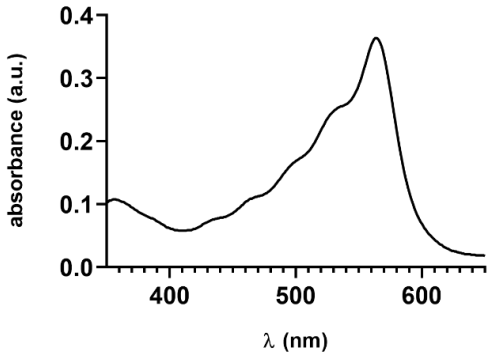

Figure S3. Absorbance spectrum of 50 µLg·mL^{-1} Rho in 1 M HCl. The maximum peak intensity was found at 564 nm and this value was selected as the excitation wavelength of fluorescence measurements.

APPENDIX IV

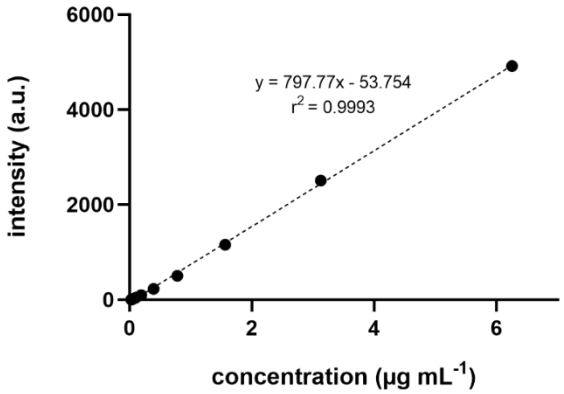

Figure S4. Fluorescence calibration curve of Rho in 1 M HCl. Samples were excited at 564 nm and the emitted intensity was read at 585 nm. The points were fit to a linear approximation.

APPENDIX V

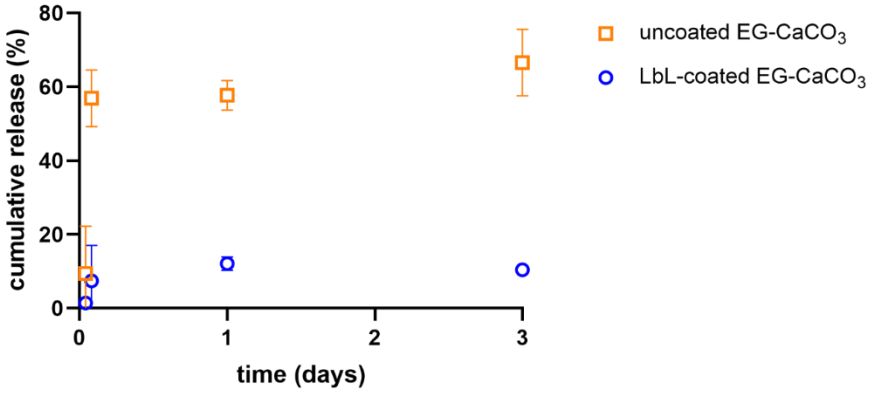

Figure S5. Cumulative release of Rho from uncoated (□) and LbL-coated EG-$CaCO_3$ (○) nanoparticles at pH 7.4 for 3 days. Data are means ± one standard deviation. Some error bars are too small to see.

APPENDIX VI

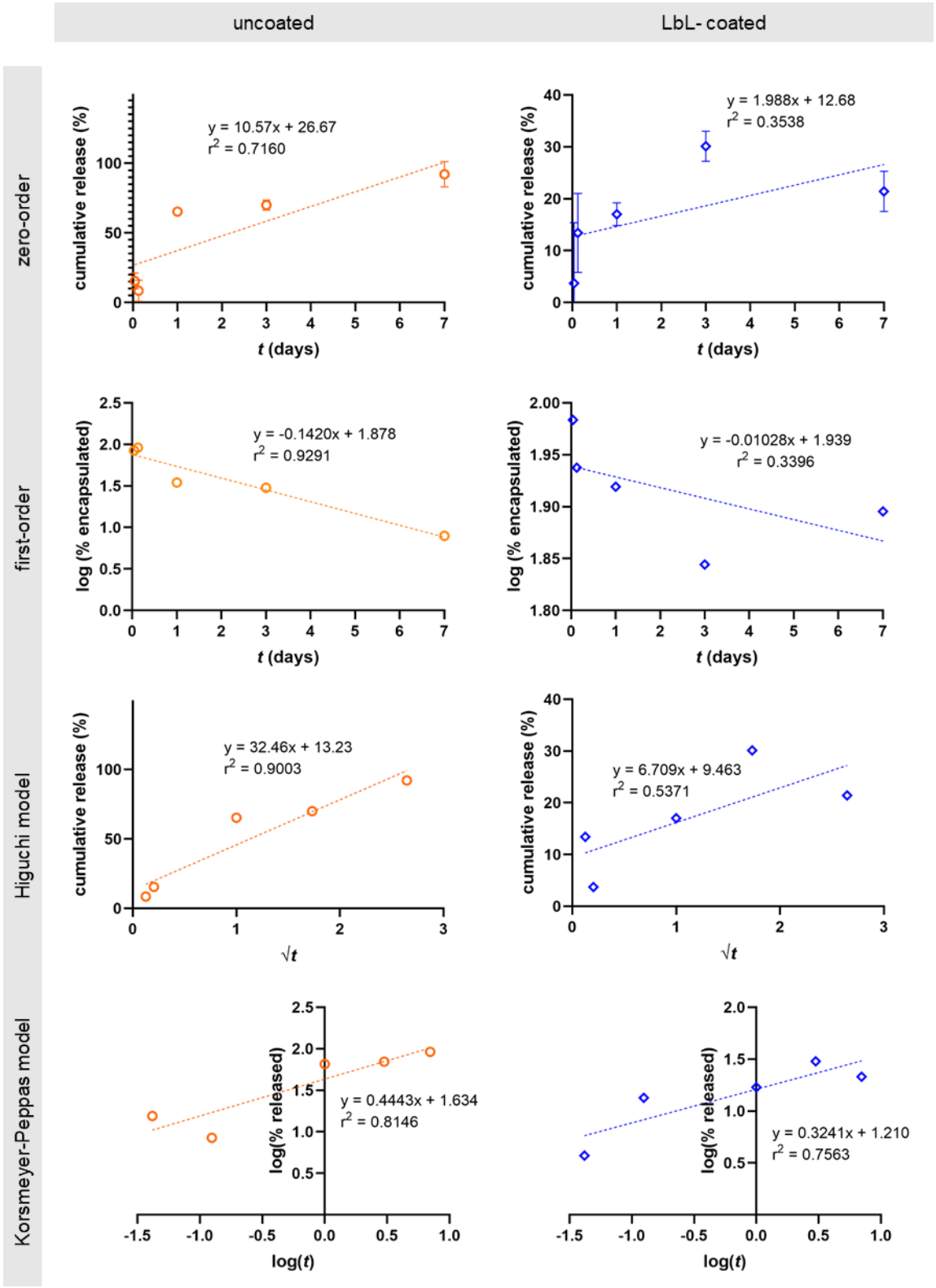

Figure S6. Analysis of the Rho release data from uncoated and coated EG-$CaCO_3$ nanoparticles approximated to the release models: zero-order (cumulative release vs time), first-order (log remaining amount vs time), Higuchi (cumulative release vs square root of time), and Korsmeyer-Peppas (log cumulative release vs log time). Fitting equations and coefficients of determination (r^2) are shown.

APPENDIX VII

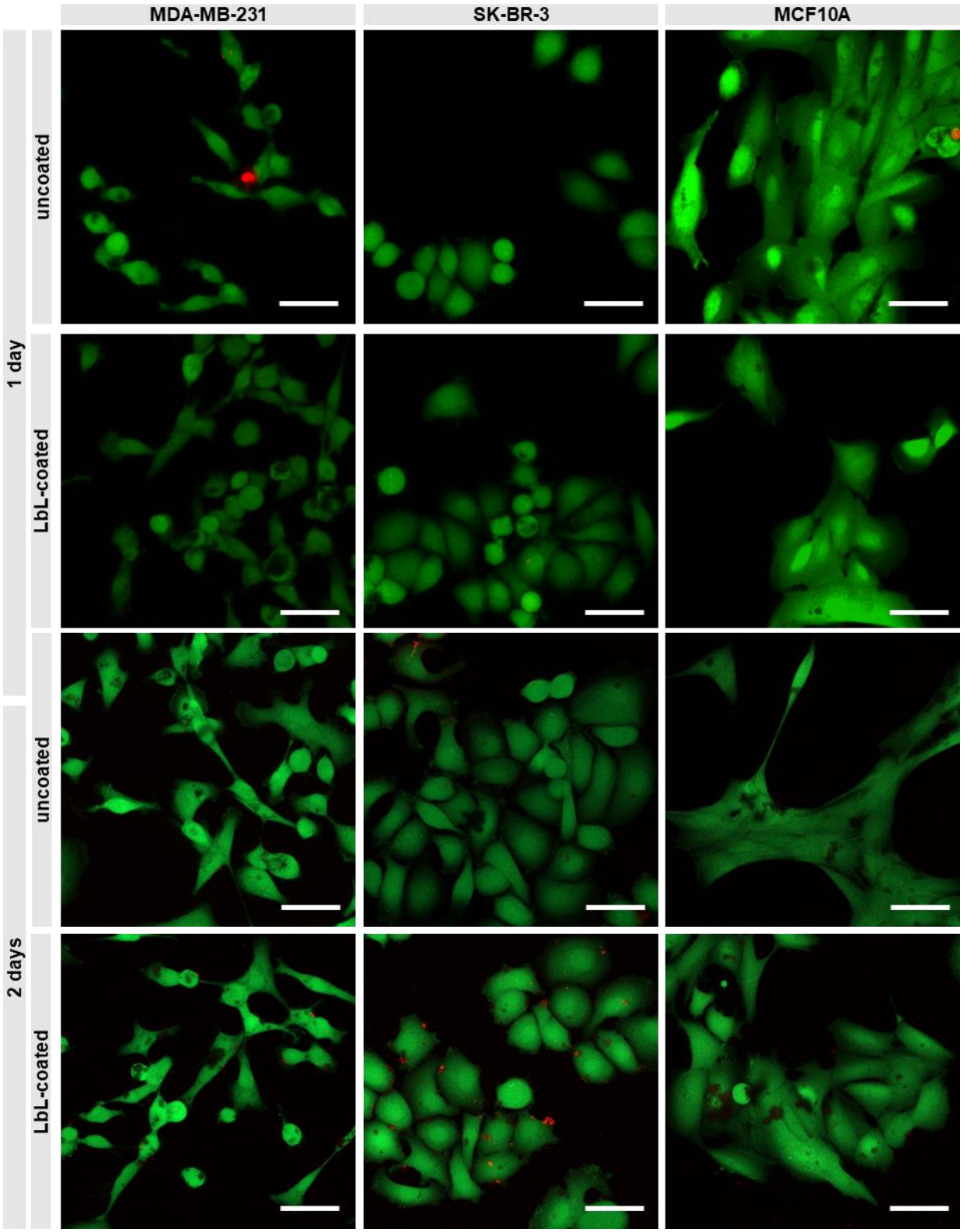

Figure S7. Live/Dead assay of MDA-MB-231, SK-BR-3, and MCF10A cell lines incubated with uncoated and LbL-coated EG-$CaCO_3$ nanoparticles for 1 and 2 days (green: live; red: dead).

APPENDIX VIII

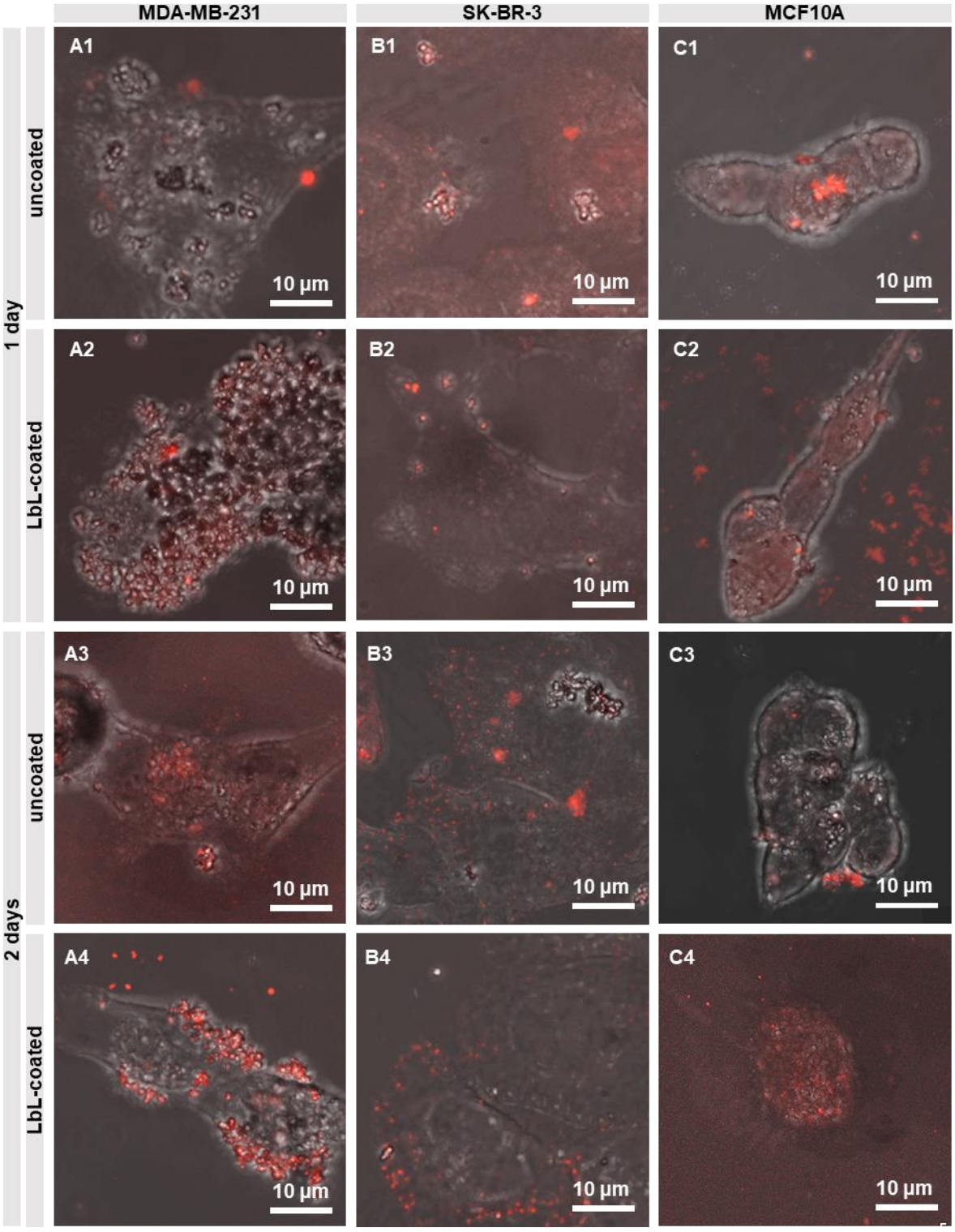

Figure S8. Distribution of uncoated (–) and LbL-coated (+) EG-$CaCO_3$ nanoparticles after 1 and 2 days of incubation with MDA-MB-231, SK-BR-3, and MCF10A cell lines (red: Rho).

APPENDIX IX

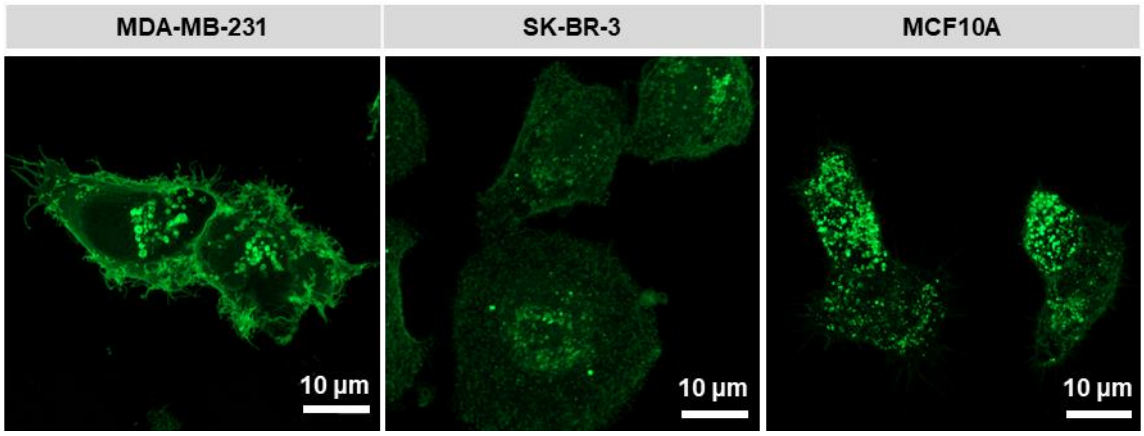

Figure S9. Staining of HA in MDA-MB-231, SK-BR-3, and MCF10A cell lines with FITC-WGA.

APPENDIX X

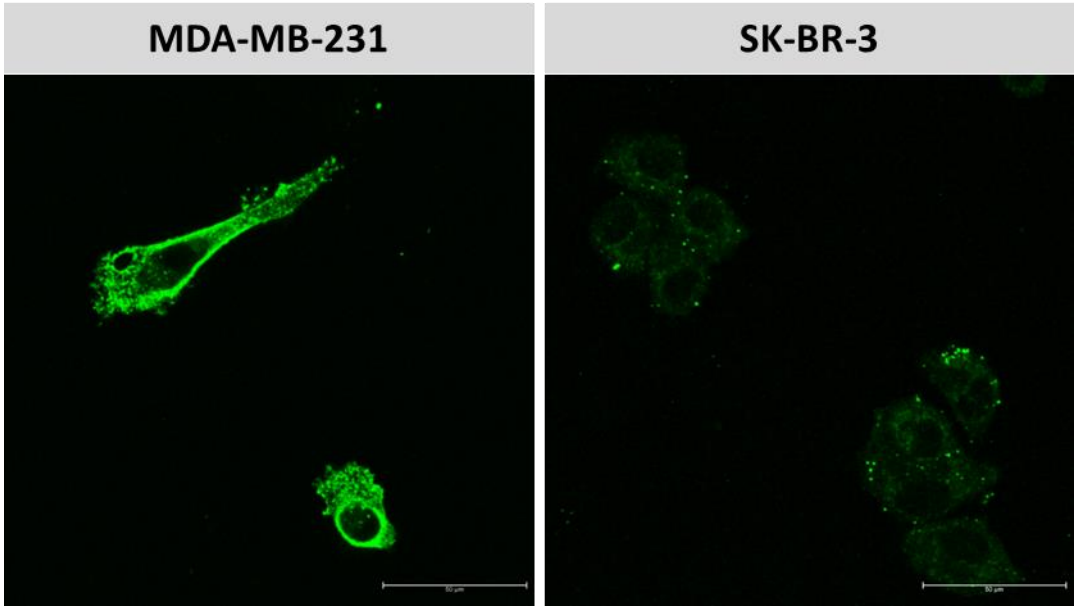

Figure S10- Hyaluronan expression in MDA-MB-231 and Sk-Br-3 cells. Endogenous hyaluronan was detetcted with biotinylated hyaluronan binding protein.followed by streptavidin-AlexaFLuor® 488.